SANDIA REPORT
SAND2014-15909
Unlimited Release
Printed July 2014

Effects of Analog-to-Digital Converter Nonlinearities on Radar Range-Doppler Maps

Armin W. Doerry, Dale F. Dubbert, and Bert L. Tise

Prepared by
Sandia National Laboratories
Albuquerque, New Mexico 87185 and Livermore, California 94550

Sandia National Laboratories is a multi-program laboratory managed and operated by Sandia Corporation, a wholly owned subsidiary of Lockheed Martin Corporation, for the U.S. Department of Energy's National Nuclear Security Administration under contract DE-AC04-94AL85000.

Issued by Sandia National Laboratories, operated for the United States Department of Energy by Sandia Corporation.

Available to DOE and DOE contractors from

U.S. Department of Energy
Office of Scientific and Technical Information
P.O. Box 62
Oak Ridge, TN 37831

Telephone: (865) 576-8401
Facsimile: (865) 576-5728
E-Mail: reports@adonis.osti.gov
Online ordering: http://www.osti.gov/bridge

Available to the public from

U.S. Department of Commerce
National Technical Information Service
5285 Port Royal Rd.
Springfield, VA 22161

Telephone: (800) 553-6847
Facsimile: (703) 605-6900
E-Mail: orders@ntis.fedworld.gov
Online order: http://www.ntis.gov/help/ordermethods.asp?loc=7-4-0#online

SAND2014-15909
Unlimited Release
Printed July 2014

Effects of Analog-to-Digital Converter Nonlinearities on Radar Range-Doppler Maps

Armin Doerry
ISR Mission Engineering

Dale Dubbert
ISR EM & Sensor Technologies

Bert Tise
ISR Real Time Processing

Sandia National Laboratories
PO Box 5800
Albuquerque, NM 87185-0519

Abstract

Radar operation, particularly Ground Moving Target Indicator (GMTI) radar modes, are very sensitive to anomalous effects of system nonlinearities. These throw off harmonic spurs that are sometimes detected as false alarms. One significant source of nonlinear behavior is the Analog to Digital Converter (ADC). One measure of its undesired nonlinearity is its Integral Nonlinearity (INL) specification. We examine in this report the relationship of INL to GMTI performance.

Acknowledgements

This report is the result of an unfunded Research and Development effort.

Sandia National Laboratories is a multi-program laboratory managed and operated by Sandia Corporation, a wholly owned subsidiary of Lockheed Martin Corporation, for the U.S. Department of Energy's National Nuclear Security Administration under contract DE-AC04-94AL85000.

Contents

“My nature is to be linear, and when I'm not, I feel really proud of myself.”
-- Cynthia Weil

Foreword

This report details the results of an academic study. It does not presently exemplify any operational systems with respect to modes, methodologies, or techniques.

Classification

The specific mathematics and algorithms presented herein do not bear any release restrictions or distribution limitations.

This distribution limitations of this report are in accordance with the classification guidance detailed in the memorandum “Classification Guidance Recommendations for Sandia Radar Testbed Research and Development”, DRAFT memorandum from Brett Remund (Deputy Director, RF Remote Sensing Systems, Electronic Systems Center) to Randy Bell (US Department of Energy, NA-22), February 23, 2004. Sandia has adopted this guidance where otherwise none has been given.

This report formalizes preexisting informal notes and other documentation on the subject matter herein.

1 Introduction

Radar data and data products often exhibit extraordinarily large dynamic ranges. Synthetic Aperture Radar (SAR) images can be well beyond 100 dB. Even Ground Moving Target Indicator (GMTI) range-Doppler maps exhibit dynamic ranges routinely above 80 dB. With GMTI data, we are often looking for small targets that manifest barely above the noise level, but still in the presence of other large target energies. This is especially true for Dismount-detection GMTI (DMTI). Achieving this level of dynamic range requires an extraordinarily linear radar channel.

One inescapably nonlinear component is the Analog to Digital Converter (ADC). The ADC's quantization function is indeed nonlinear, but can be readily accommodated if it exhibits known (generally uniform) quantization steps. However, if the quantization steps are unknown, that is other than that which is presumed, albeit usually bounded to some fraction of the nominal quantization step size, then we might expect anomalous effects in the radar data. This typically will manifest as undesirable harmonic spurs in the range-Doppler map, leading to increased false alarms and reduced detection probability for GMTI operation.

The unknown and undesired nonlinearity aspects of an ADC are embodied in the ADC's Differential Nonlinearity (DNL) and its Integral Nonlinearity (INL) specifications. Inadequate performance in this regard can be particularly problematic for GMTI operation, and is in fact not uncommon. GMTI modes are particularly sensitive because we are often trying to detect very weak targets against the noise floor of the radar.

Other component specifications also address ADC nonlinearity.[1]

What follows is an analysis of INL effects, as manifests in a range-Doppler map, with the assumption of stretch processing having been employed.[2] We will further assume IF sampling with digital down-conversion, a common technique for high-performance radar systems.

“Have no fear of perfection - you'll never reach it.”
— Salvador Dalí

2 Discussion – Integral Nonlinearity

A good primer on Integral Nonlinearity (INL) is an Application Note by Maxim Integrated Products, Inc.[3]

2.1 What is it?

The ideal transfer function for an ADC is a stair-step function, where ADC codes exhibit constant increments with uniform step sizes in input voltage. Quantization is said to be uniform. The centers of such steps are linear, that is, on a straight line.

Alas, real ADCs exhibit steps that are not on a straight line. We don't like this, but that's just the way it is. We do like ADC components that minimize nonlinear behavior.

The nonuniformity of the individual steps are recorded as a Differential Nonlinearity (DNL). The accumulation of the nonlinear steps indicate the departure of the actual ADC transfer function from a straight line, and is recorded as the Integral Nonlinearity (INL).

Both INL and DNL are typically reported as fractions of the Least-Significant Bit (LSB) of the ADC. They may also be reported as fractions or percent of Full Scale Range (FSR). It is particularly important to remember that that the LSB metric in absolute terms does in fact depend on the number of bits in the ADC.

Nevertheless, INL and DNL are simply measures of the nonlinear behavior of the ADC, beyond merely sampling and quantizing the data in a uniform fashion.

Measurement of INL and DNL is addressed in an Application Note from Analog Devices.[4]

2.2 How Does it Manifest in the Sampled Data?

This is all about relating an INL spec to ADC sample values in a mathematical sense.

2.2.1 Digital Down-Conversion – Ideal ADC

We begin with a single ADC operating at some sampling frequency defined as

f_S = ADC sampling frequency. (1)

The sample period is the inverse of this, namely

$T_S = 1/f_S$ = ADC fast-time sample period. (2)

It is particularly convenient for the input signal to be at an IF center frequency of $f_S/4$. Consequently, we identify the IF signal as

$$x_{IF}(t) = x(t)e^{j2\pi(f_s/4)t} + x^*(t)e^{-j2\pi(f_s/4)t}. \quad (3)$$

Note that this signal is real-valued. Furthermore, $x(t)$ is typically band-limited to something less than $f_S/2$, and often to less than $f_S/4$.

The ADC samples this signal at uniformly spaced sample times of

$$t = T_S n, \quad (4)$$

and generates data samples ideally described by

$$x_{ADC}(n) = x_{IF}(T_S n), \quad (5)$$

where

n = sample index value. (6)

Note that $x_{ADC}(n)$ is also real-valued.

The digital down-conversion is typically implemented as the complex multiplication

$$x_{dem}(n) = e^{-j(\pi/2)n}\left[x_{ADC}(n)\right]. \quad (7)$$

Combining the previous results yields the signal of interest, namely

$$x_{dem}(n) = x(T_S n) + x^*(T_S n)e^{-j\pi n}. \quad (8)$$

This normally undergoes additional low-pass filtering to remove the $e^{-j\pi n}$ modulated term, and typically some data decimation as well. We model the demodulated and filtered signal as

$$x_{demfil}(n) = x_{dem}(n) * h_{demfil}(n) \approx x(T_s n) \ , \tag{9}$$

where

$h_{demfil}(n)$ = the demodulator filter. (10)

It is this term $x_{demfil}(n) \approx x(n/f_s)$ that is of interest to us for further processing.

2.2.2 Digital Down-Conversion – ADC With INL

The development begins as in the previous section, but departs at the point of describing the ADC samples. The new description includes an error term due to INL. That is

$$x_{ADC}(n) = x_{IF}(T_s n) + \varepsilon_{INL}\left(x_{IF}(T_s n)\right), \tag{11}$$

where

$\varepsilon_{INL}(z)$ = the error added to the ideal signal due to INL. (12)

We note that the error in $x_{ADC}(n)$ depends on the instantaneous value for $x_{ADC}(n)$ itself. Ideally, we desire $\varepsilon_{INL}(z) = 0$. Failing that, we desire the effects of $\varepsilon_{INL}(z)$ be negligible in the range-Doppler map, especially in GMTI modes.

As before, the digital down-conversion is implemented as the complex multiplication

$$x_{dem}(n) = e^{-j(\pi/2)n}\left[x_{ADC}(n)\right]. \tag{13}$$

Combining the previous results yields the signal of interest, namely

$$x_{dem}(n) = \left[x(T_s n) + x^*(T_s n)e^{-j\pi n} + e^{-j(\pi/2)n}\varepsilon_{INL}\left(x_{IF}(T_s n)\right)\right]. \tag{14}$$

This normally undergoes additional low-pass filtering to remove the $e^{-j\pi n}$ modulated term, and typically some data decimation as well. We again model the filtered signal as

$$x_{demfil}(n) = x_{dem}(n) * h_{demfil}(n). \tag{15}$$

Expanding this yields

$$x_{demfil}(n) \approx x(T_s n) + \left[\left\{ e^{-j(\pi/2)n} \varepsilon_{INL}\left(x_{IF}(T_s n) \right) \right\} * h_{demfil}(n) \right]. \quad (16)$$

The term within the square brackets represents the impact of INL on the data. Some comments are in order

- The INL affects the data generally in an annoyingly nonlinear fashion. Therein lays the problem.
- The nonlinear function is the calculation of $\varepsilon_{INL}(x_{IF}(T_s n))$. After that, all operations are linear again.
- The effects of INL of consequence are those that make it through the filter $h_{demfil}(n)$, after a frequency shift by $e^{-j(\pi/2)n}$. If the filter were perfect, then it is only the INL effects that make it through the passband. Otherwise, we also need to include perhaps effects that are significant even after stopband attenuation.

2.2.3 Details of Signal Conversion – Ideal ADC

In the foregoing analysis, we have assumed that the ideal conversion was the assignment of sample values based on

$$x_{ADC}(n) = x_{IF}(T_s n). \quad (17)$$

We now explore this in somewhat more detail.

We shall assume that the ADC conversion range is limited to the region

$$-1/2 \le x_{IF}(T_s n) < 1/2. \quad (18)$$

However, the ADC conversion function operates on some range of voltages, and assigns output code values consistent with

$$\begin{aligned} &0 \text{ for the most negative signal value, and} \\ &2^{b_{ADC}} - 1 \text{ for the most positive signal value,} \end{aligned} \quad (19)$$

where

$$b_{ADC} = \text{number of bits in the ADC.} \quad (20)$$

The ADC output is quantized to $2^{b_{ADC}}$ different values, hopefully with constant step sizes. We define the conversion operation with the function

$$Z = Q\left(z, b_{ADC}\right), \tag{21}$$

where

z = analog input with range $0 \le z < 1$, and
Z = assigned quantized output with range $0 \le Z < 1$. (22)

We also define the ideal uniform quantization step size then as

$$q = 2^{-b_{ADC}}. \tag{23}$$

The conversion operation in practice produces a quantization error. That is, for an ideal ADC, this error is

$$\varepsilon_q\left(z, b_{ADC}\right) = Z - z. \tag{24}$$

The transfer function is defined to be linear and without error when

$$\varepsilon_q\left(kq, b_{ADC}\right) = 0, \tag{25}$$

where

k = integer, that is $k \in I$, and $0 \le k < 2^{b_{ADC}}$. (26)

Consequently, we can infer that for an ideal ADC,

$$Q\left(kq, b_{ADC}\right) - kq = 0. \tag{27}$$

We note that in this case

$$-q/2 \le \varepsilon_q\left(z, b_{ADC}\right) < q/2. \tag{28}$$

For complex (in the 'complicated' sense) signals, this error is uniformly distributed, and uncorrelated (white). We like this, and strive to make this happen even for low-level signals with dither signals.

Given all this, we can relate a more accurate ideal conversion operation as

$$x_{ADC}\left(n\right) = x_{IF}\left(T_s n\right) + \varepsilon_q\left(\left(x_{IF}\left(T_s n\right) + \frac{1}{2}\right), b_{ADC}\right). \tag{29}$$

However, statistically, since the average quantization error is zero, we can generally presume

$$x_{ADC}\left(n\right) = x_{IF}\left(T_s n\right). \tag{30}$$

2.2.4 Details of Signal Conversion – ADC with INL

In the previous development for an ideal ADC, we stipulated that the quantization error

$$\varepsilon_q\left(kq, b_{ADC}\right) = 0\,. \tag{31}$$

We now depart from this assumption, and allow that

$$\varepsilon_q\left(kq, b_{ADC}\right) \neq 0\,. \tag{32}$$

In particular, we identify the residual error as its own function

$$\varepsilon_q\left(kq, b_{ADC}\right) = g\left(kq\right). \tag{33}$$

We identify the nature of $g(kq)$ to be a smoothed residual error, that is, interpolated between sample values of argument (kq). Recall that the general quantization error will be a stair-step function for a continuum of ADC input values. An important distinction is

$$\begin{aligned} &\varepsilon_q(z, b_{ADC}) \text{ = stair-step function (albeit with perhaps nonuniform steps),} \\ &g(z) \text{ = interpolated residual error.} \end{aligned} \tag{34}$$

The equality of these two holds only at argument values $z = kq$.

We define a new error as

$$\varepsilon_{q'}\left(z, b_{ADC}\right) = \varepsilon_q\left(z, b_{ADC}\right) - g\left(z\right). \tag{35}$$

Of course, this new error behaves more like the quantization error from an ideal ADC. That is, it exhibits a stair-step behavior with

$$\varepsilon_{q'}\left(kq, b_{ADC}\right) = 0\,. \tag{36}$$

Nevertheless, the actual quantization error is now the sum of this idealized quantization error and the interpolated residual error, that is

$$\varepsilon_q\left(z, b_{ADC}\right) = \varepsilon_{q'}\left(z, b_{ADC}\right) + g\left(z\right). \tag{37}$$

Given all this, we identify our new conversion operation as

$$x_{ADC}\left(n\right) = x_{IF}\left(T_s n\right) + \varepsilon_{q'}\left(\left(x_{IF}\left(T_s n\right) + \frac{1}{2}\right), b_{ADC}\right) + g\left(x_{IF}\left(T_s n\right) + \frac{1}{2}\right). \tag{38}$$

However, as before, the idealized quantization error is statistically zero, so we can generally presume

$$x_{ADC}(n) = x_{IF}(T_s n) + g\left(x_{IF}(T_s n) + \frac{1}{2} \right). \tag{39}$$

With respect to the earlier development, we identify the INL error as

$$\varepsilon_{INL}\left(x_{IF}(T_s n) \right) = g\left(x_{IF}(T_s n) + \frac{1}{2} \right). \tag{40}$$

More commonly, an INL specification will present a sample plot with abscissa units between zero and full-scale, and ordinate units of Least Significant Bit (LSB). We identify such a function as

$$G(w) = \text{typical INL specification, in units of LSB,} \tag{41}$$

where

$$\begin{aligned} w &= \text{abscissa, with } 0 \le w < fs, \\ fs &= \text{full-scale value of ADC input (not to be confused with sampling frequency).} \end{aligned} \tag{42}$$

We relate the typical INL specification to the functions we are interested in via

$$g(z) = q\, G(z\ fs). \tag{43}$$

More specifically, the INL error in terms of the INL specification as

$$\varepsilon_{INL}\left(x_{IF}(T_s n) \right) = q\, G\left(\left(x_{IF}(T_s n) + \frac{1}{2} \right) fs \right). \tag{44}$$

We note the following important points.

- The effects of INL depend not only on the component INL specification in terms of LSB, but also on the quantization step size, i.e., the number of bits in the ADC.
- When comparing different ADC components, their INL specifications need to be 'normalized' with respect to the quantization step size q. That is, the proper comparison is $\varepsilon_{INL}(\,)$, and not $G(\,)$.

2.2.5 Effects of Nonlinearities on Signals

The question we answer next is "Given some INL specification $G(\,)$, and some input $x_{IF}(\,)$, what does it really do to $\varepsilon_{INL}(\,)$?"

For convenience, we shall hereafter presume the ADC full-scale $fs = 1$.

It also becomes convenient to expand the INL specification into a Taylor Series about its mid-range. This yields

$$G(z) = G\left(\frac{1}{2}\right) + \frac{G'\left(\frac{1}{2}\right)}{1}\left(z-\frac{1}{2}\right) + \frac{G''\left(\frac{1}{2}\right)}{2}\left(z-\frac{1}{2}\right)^2 + \frac{G'''\left(\frac{1}{2}\right)}{6}\left(z-\frac{1}{2}\right)^3 + \ldots . \quad (45)$$

Note that this is just a polynomial fit to the data, that is

$$G(z) = G_0 + G_1\left(z-\frac{1}{2}\right) + G_2\left(z-\frac{1}{2}\right)^2 + G_3\left(z-\frac{1}{2}\right)^3 + \ldots + G_m\left(z-\frac{1}{2}\right)^m + \ldots , \quad (46)$$

where

$$G_m = \frac{1}{m!}\frac{d^m}{dz^m}G(z)\bigg|_{z=1/2} = \text{constant coefficients.} \quad (47)$$

This allows the INL error to be written as

$$\varepsilon_{INL}\left(x_{IF}\left(T_s n\right)\right) = \begin{bmatrix} qG_0 \\ +qG_1\left(x_{IF}\left(T_s n\right)\right) \\ +qG_2\left(x_{IF}\left(T_s n\right)\right)^2 \\ +qG_3\left(x_{IF}\left(T_s n\right)\right)^3 \\ +\ldots \end{bmatrix} = \sum_{m=0}^{\infty} qG_m\left(x_{IF}\left(T_s n\right)\right)^m . \quad (48)$$

So, INL causes the addition of powers of the input signal. This is, as one might expect, a nonlinear function, so scaling and superposition do not hold.

The constant term represents a bias. The linear term ultimately affects the scaling of the data. The problematic terms are the quadratic and higher-order terms, as they embody the nonlinearities that are particularly troublesome. Fortunately they are generally pretty small, but not without significance.

Recall that $x_{IF}(T_s n)$ is real-valued. We shall presume that the input is a single-frequency sinusoid described by

$$x_{IF}\left(T_s n\right) = A\cos\left(2\pi\left(f_d + \frac{f_s}{4}\right)T_s n\right), \quad (49)$$

where

f_d = modulation frequency offset from the IF carrier, and
A = amplitude of IF signal. (50)

Note that $|A| \le 1/2$, but is typically much smaller. Note again that for digital down-conversion we enjoy the IF carrier at $f_s/4$.

Clearly, powers of this signal yield

$$\left(x_{IF}\left(T_s n\right)\right)^m = A^m \cos^m\left(2\pi\left(f_d + \frac{f_s}{4}\right)T_s n\right). \tag{51}$$

We recall the trig identity

$$\cos^m(\theta) = \begin{cases} \dfrac{2}{2^m}\displaystyle\sum_{k=0}^{\frac{m-1}{2}} \binom{m}{k}\cos\left((m-2k)\theta\right) & m \text{ odd} \\ \dfrac{1}{2^m}\binom{m}{m/2} + \dfrac{2}{2^m}\displaystyle\sum_{k=0}^{\frac{m}{2}-1}\binom{m}{k}\cos\left((m-2k)\theta\right) & m \text{ even} \end{cases}. \tag{52}$$

In particular, some examples include

$$\begin{aligned} \cos^2(\theta) &= \frac{1}{2} + \frac{1}{2}\cos(2\theta), \\ \cos^3(\theta) &= \frac{3}{4}\cos(\theta) + \frac{1}{4}\cos(3\theta), \\ \cos^4(\theta) &= \frac{3}{8} + \frac{1}{2}\cos(2\theta) + \frac{1}{8}\cos(4\theta), \text{ and} \\ \cos^5(\theta) &= \frac{5}{8}\cos(\theta) + \frac{5}{16}\cos(3\theta) + \frac{1}{16}\cos(5\theta). \end{aligned} \tag{53}$$

Several important points are worth noting.

- The expansion of $A^m \cos^m(\theta)$ contains a term $\left(A^m/2^{m-1}\right)\cos(m\theta)$.
- That is, $\cos^m(\theta)$ contains phase (and frequency) multiples of θ up to $m\theta$.
- Higher order terms (larger values for *m*) generally contribute lesser amounts of energy, differences in G_m notwithstanding.

This suggests that we can equate

$$\sum_{m=0}^{M} G_m A^m \cos^m(\theta) = \sum_{m=0}^{M} C_m(A)\cos(m\theta), \tag{54}$$

where

$$\begin{aligned} M &= \text{the maximum value for } m \text{ for which we have interest,} \\ C_m(A) &= \text{polynomial function of } A, \text{ for the } m^{\text{th}} \text{ harmonic.} \end{aligned} \tag{55}$$

We can calculate the $C_m(A)$ by noting that

$$\sum_{m=0}^{M} G_m A^m \cos^m(\theta) = \begin{cases} \displaystyle\sum_{m=0}^{M} G_m A^m \frac{2}{2^m} \sum_{k=0}^{\frac{m-1}{2}} \binom{m}{k} \cos\big((m-2k)\theta\big) & m \text{ odd} \\ \displaystyle\sum_{m=0}^{M} G_m A^m \left(\frac{1}{2^m}\binom{m}{m/2} + \frac{2}{2^m} \sum_{k=0}^{\frac{m}{2}-1} \binom{m}{k} \cos\big((m-2k)\theta\big) \right) & m \text{ even} \end{cases}. \tag{56}$$

By substituting $(m-2k) = (2p+1)$ for odd m, and $(m-2k) = (2p)$ for even m, we can calculate

$$\sum_{m=0}^{M} G_m A^m \cos^m(\theta) = \left\{ \begin{array}{l} \displaystyle\sum_{n=0}^{M/2} G_{2n} A^{2n} \frac{1}{2^{2n}} \binom{m}{n} \\ \displaystyle + \sum_{p=0}^{(M-1)/2} \left[\sum_{n=p}^{(M-1)/2} G_{2n+1} A^{2n+1} \frac{2}{2^{2n+1}} \binom{2n+1}{n-p} \right] \cos\big((2p+1)\theta\big) \\ \displaystyle + \sum_{p=1}^{M/2} \left[\sum_{n=p}^{M/2} G_{2n} A^{2n} \frac{2}{2^{2n}} \binom{2n}{n-p} \right] \cos(2p\theta) \end{array} \right\}. \tag{57}$$

From this we recognize

$$C_m(A)=\begin{cases}\displaystyle\sum_{n=0}^{M/2} G_{2n}A^{2n}\frac{1}{2^{2n}}\binom{2n}{n} & m=0\\ \displaystyle\sum_{n=p}^{(M-1)/2} G_{2n+1}A^{2n+1}\frac{2}{2^{2n+1}}\binom{2n+1}{n-p} & m=(2p+1)\geq 1\cdot\\ \displaystyle\sum_{n=p}^{M/2} G_{2n}A^{2n}\frac{2}{2^{2n}}\binom{2n}{n-p} & m=2p\geq 2\end{cases} \tag{58}$$

This is illustrated by putting some of this together. We examine the first seven terms of the polynomial expansion, and calculate

$$\sum_{m=0}^{7} G_m A^m\cos^m(\theta)=\left\{\begin{aligned}&\left(G_0+\frac{1}{2}G_2A^2+\frac{3}{8}G_4A^4+\frac{5}{16}G_6A^6\right)\\&+\left(G_1A+\frac{3}{4}G_3A^3+\frac{5}{8}G_5A^5+\frac{35}{64}G_7A^7\right)\cos(\theta)\\&+\left(\frac{1}{2}G_2A^2+\frac{1}{2}G_4A^4+\frac{15}{32}G_6A^6\right)\cos(2\theta)\\&+\left(\frac{1}{4}G_3A^3+\frac{5}{16}G_5A^5+\frac{21}{64}G_7A^7\right)\cos(3\theta)\\&+\left(\frac{1}{8}G_4A^4+\frac{3}{16}G_6A^6\right)\cos(4\theta)\\&+\left(\frac{1}{16}G_5A^5+\frac{7}{64}G_7A^7\right)\cos(5\theta)\\&+\left(\frac{1}{32}G_6A^6\right)\cos(6\theta)\\&+\left(\frac{1}{64}G_7A^7\right)\cos(7\theta)\end{aligned}\right\}. \tag{59}$$

This expansion clearly illustrates the very important point that the coefficients of $\cos(m\theta)$ are themselves polynomials of amplitude A. Even for very small *m*, the polynomials would be of exceptionally large order. This of course implies that the coefficient of any particular $\cos(m\theta)$ will observe polynomial behavior as a function of *A*. That is, as amplitude *A* increases, the coefficient of any particular $\cos(m\theta)$ may increase, decrease, or disappear entirely. That is, the coefficient of any particular $\cos(m\theta)$ is not only nonlinear with respect *A*, it may not be even monotonic with respect to *A*.

The bottom line is that, for time-varying θ, the relative strength of a particular harmonic may be highly dependent on the amplitude of the input signal.

We summarize the above by noting that for input signal

$$x_{IF}\left(T_s n\right) = A\cos\left(2\pi\left(f_d + \frac{f_s}{4}\right)T_s n\right), \tag{60}$$

we identify the error due to INL for this sinusoidal input as

$$\begin{aligned}&\varepsilon_{INL}\left(A\cos\left(2\pi\left(f_d + \frac{f_s}{4}\right)T_s n\right)\right),\\ &= q\sum_{m=0}^{\infty} G_m A^m \cos^m\left(2\pi\left(f_d + \frac{f_s}{4}\right)T_s n\right) = q\sum_{m=0}^{\infty} C_m\left(A\right)\cos\left(2\pi m\left(f_d + \frac{f_s}{4}\right)T_s n\right).\end{aligned} \tag{61}$$

We observe the following.

- Any particular $C_m(A)$ contains no terms of lower order than A^m. So, other things equal, $C_m(A)$ are likely smaller for larger *m*. However, there is no guarantee that other things are equal.

- Every instance of A^m is multiplied by G_m.

- We expect that of particular concern will be large values of G_m for low order *m*. This implies a concern for large low-frequency structure to the INL characteristic.

- Since G_m are based on a function with units *LSB*, the impact on INL error clearly depends on the number of bits in the ADC.

- The largest undesired harmonic is that for which $C_m(A)$ is the greatest, over all amplitudes *A* for $0 \le A \le 1/2$ and for all $m \ge 2$.

- It is not just the peak deviation of the INL that is of concern. The underlying structure of the INL characteristic will substantially affect the nature of the harmonic content in the data.

- We reiterate an earlier point in observing that when comparing different ADC components, their INL specifications need to be 'normalized' with respect to the quantization step size *q*. That is, the proper comparison is the error $\varepsilon_{INL}(\,)$, and not the direct component specification $G(\,)$.

We also remind ourselves that insofar as the largest impact on the ultimate data, we need to take into account any attenuation by the bandwidth reduction filtering subsequent to data sampling. We will examine this in more detail later.

2.2.6 INL Analysis Based on Energy

We now investigate the total energy in the INL distortion as generated by a sinusoidal tone.

We shall again presume that the input is a sinusoidal tone, namely

$$x_{IF}\left(T_s n\right) = A\cos\left(\omega_n n\right), \tag{62}$$

where for notational convenience we use the substitution

$$\omega_n = 2\pi\left(f_d + \frac{f_s}{4}\right)T_s, \tag{63}$$

The INL distortion is then given as

$$\varepsilon_{INL}\left(A\cos\left(\omega_n n\right)\right) = qG\left(A\cos\left(\omega_n n\right) + \frac{1}{2}\right). \tag{64}$$

Consequently the net distorted signal is sum of the original signal with its distortion component, that is

$$x_{ADC}\left(n\right) = A\cos\left(\omega_n n\right) + qG\left(A\cos\left(\omega_n n\right) + \frac{1}{2}\right). \tag{65}$$

We note that the INL distortion component generally adds power to the output signal. While it does in fact modify the power at the fundamental frequency by some small amount, it also adds power at other frequencies, including zero-frequency or DC. While we are most interested in power at higher harmonics of the fundamental, this power is bounded by the total power in the INL distortion component.

We calculate the power in the INL distortion component as

$$P_{INL} = q^2\,\mathrm{mean}\left\{G^2\left(A\cos\left(\omega_n n\right) + \frac{1}{2}\right)\right\}. \tag{66}$$

Of course, the power in the desired signal is

$$P_0 = \mathrm{mean}\left\{A^2\cos^2\left(\omega_n n\right)\right\} = \frac{A^2}{2}. \tag{67}$$

The relative INL distortion power level for a sinusoidal signal is then their ratio, or

$$\frac{P_{INL}}{P_0} = 2\frac{q^2}{A^2}\,\mathrm{mean}\left\{G^2\left(A\cos\left(\omega_n n\right) + \frac{1}{2}\right)\right\}. \tag{68}$$

2.2.7 Effects on Doppler

We return to the expression for INL, but this time in terms of a generic phase,

$$\varepsilon_{INL}\left(A\cos\left(\theta\right)\right) = q\sum_{m=0}^{\infty} G_m A^m \cos^m\left(\theta\right) = q\sum_{m=0}^{\infty} C_m\left(A\right)\cos\left(m\theta\right). \tag{69}$$

In a range-Doppler image formed from data using stretch processing, signal frequency corresponds to range, and a pulse-to-pulse phase change corresponds to range-rate, or Doppler. A harmonic multiplies phase. Consequently, a harmonic of order *m* yields both a frequency multiple with factor *m* as well as a phase-rate multiple with factor *m*.

That is, the m^{th} harmonic of the fundamental signal is scaled and hence shifted in both frequency and Doppler. In a range-Doppler map, it will be offset in both range *and* Doppler. In a SAR image, a Doppler offset corresponds to an azimuth position offset, whereas in a GMTI map, a Doppler offset corresponds to a velocity offset.

The bottom line is that a INL spur can manifest literally all (anywhere) over the map.

2.3 INL Function Examples

We now examine some contrived examples. Unless noted otherwise, we will assume an 8-bit ADC with a peak INL of ½ LSB. Nevertheless, for 8 bits, we identify $q = 1/256$.

We will also assume 10,000 samples of a sinusoidal input with amplitude $A = 0.4$ and no noise beyond quantization. A –70 dB Taylor (nbar = 11) window function was used to push down sidelobes for spectrum calculations and observation.

2.3.1 Quadratic INL Function

Consider the contrived INL function

$$G(z) = 4\left(z - \frac{1}{2}\right)^2 - \frac{1}{2}. \tag{70}$$

This is illustrated in Figure 1. Note that for this function

$$\begin{aligned} &G(0) = 1/2, \\ &G(1/2) = -1/2, \\ &G(1) = 1/2. \end{aligned} \tag{71}$$

More generally, as desired the specification is bounded to

$$|G(z)| \le 1/2 \quad \text{for all } 0 \le z < 1. \tag{72}$$

From this we calculate

$$\begin{aligned} &G_0 = -1/2, \text{ and} \\ &G_2 = 4. \end{aligned} \tag{73}$$

All other G_m are zero. Of these, we only really care about the nonlinear term, specifically $C_2(A)$ for which $G_2 = 4$.

For this example, we select the input to be a sinusoid which we model as

$$x_{IF}(T_s n) = A\cos\left(2\pi\left(f_d + \frac{f_s}{4}\right)T_s n\right). \tag{74}$$

The INL error is then calculated as

$$\varepsilon_{INL}\left(x_{IF}(T_s n)\right) = qG_2\left(x_{IF}(T_s n)\right)^2, \tag{75}$$

or more specifically

$$\varepsilon_{INL}\left(x_{IF}\left(T_s n\right)\right)=\left[qC_0\left(A\right)+qC_2\left(A\right)\cos\left(4\pi\left(f_d+\frac{f_s}{4}\right)T_s n\right)\right], \tag{76}$$

or more specifically yet

$$\varepsilon_{INL}\left(x_{IF}\left(T_s n\right)\right)=\left[q\left(G_0+\frac{1}{2}G_2A^2\right)+q\left(\frac{1}{2}G_2A^2\right)\cos\left(4\pi\left(f_d+\frac{f_s}{4}\right)T_s n\right)\right]. \tag{77}$$

We identify the power in the desired signal as

$$P_0=\frac{A^2}{2}. \tag{78}$$

We identify the power in the undesired harmonic due to INL as

$$P_2=\frac{\left(qC_2\left(A\right)\right)^2}{2}=\frac{\left(q\frac{1}{2}G_2A^2\right)^2}{2}. \tag{79}$$

The relative spur power level is then the ratio of the two, namely

$$\frac{P_2}{P_0}=\left(\frac{qC_2\left(A\right)}{A}\right)^2=\left(\frac{qG_2A}{2}\right)^2=\left(\frac{A}{128}\right)^2. \tag{80}$$

For an input amplitude of $A=0.4$, we calculate

$$\frac{P_2}{P_0}=\left(\frac{0.4}{128}\right)^2=9.77\times10^{-6}. \tag{81}$$

This equates to −50 dBc.

So, for a quadratic INL with peak value of ½ LSB, and an input signal with $A=0.4$, this generates a second harmonic at a level of −50 dBc. A simulation of this example is illustrated in Figure 2. The spur in fact is measured in this plot at −50 dBc as predicted. Looking ahead, this is in fact judged unacceptably high for GMTI applications.

The INL distortion total energy calculates to −48 dBc. This compares to the −50 dBc calculated above for the second harmonic. The difference is due to a strong DC component.

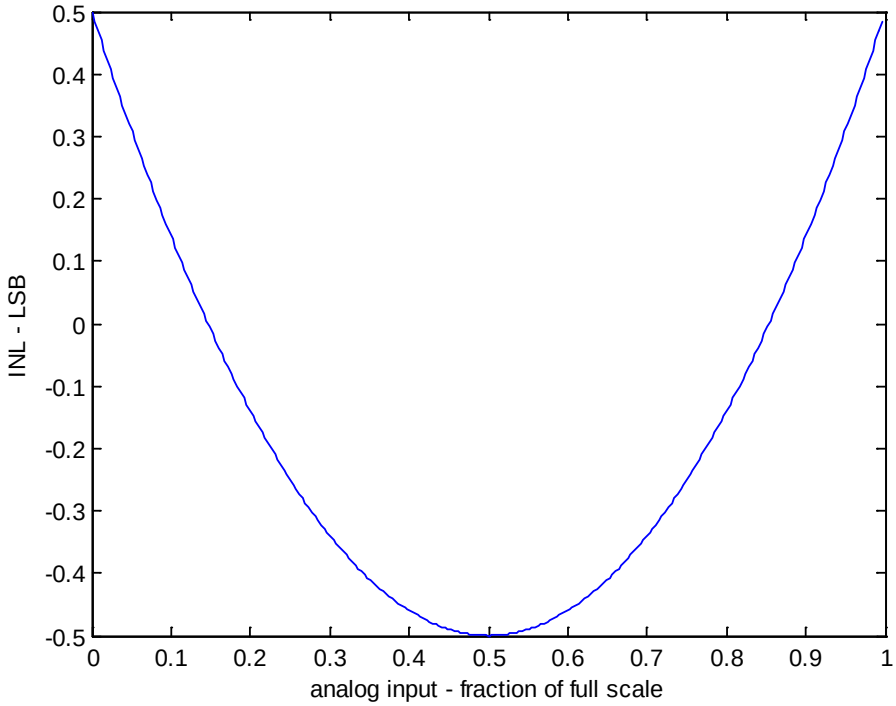

Figure 1. Example quadratic INL characteristic.

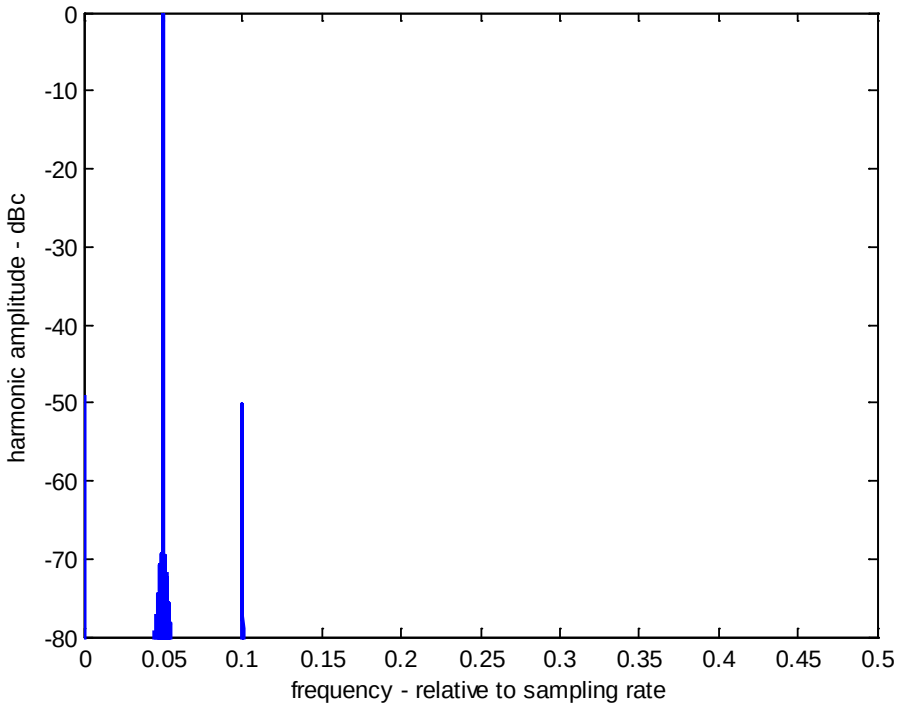

Figure 2. Spectrum of harmonic distortion.

2.3.2 Sinusoidal INL Function

Now consider the INL function with a sinusoidal characteristic, namely

$$G(z) = 0.5 \sin\left(2\pi \left(z - \frac{1}{2} \right) \right). \tag{82}$$

We can approximate this with a polynomial expansion as

$$G(z) \approx 0.5 \left[2\pi \left(z - \frac{1}{2} \right) - \frac{(2\pi)^3}{6} \left(z - \frac{1}{2} \right)^3 + \frac{(2\pi)^5}{120} \left(z - \frac{1}{2} \right)^5 - \frac{(2\pi)^7}{5040} \left(z - \frac{1}{2} \right)^7 \right]. \tag{83}$$

Both the INL and its approximation are illustrated in Figure 3. They are pretty close. From this we calculate

$$\begin{aligned} G_1 &= \pi \approx 3.14, \\ G_3 &= -\frac{(2\pi)^3}{12} \approx -20.7, \\ G_5 &= \frac{(2\pi)^5}{240} \approx 40.8, \text{ and} \\ G_7 &= -\frac{(2\pi)^7}{10080} \approx -38.4. \end{aligned} \tag{84}$$

All other G_m are presumed to be zero. Of these, we only really care about the nonlinear terms, specifically those for which $m \geq 2$. For these terms, the appropriate coefficients are calculated for a signal amplitude $A = 0.4$ as

$$\begin{aligned} C_3(A) &\approx \left(\frac{1}{4} G_3 A^3 + \frac{5}{16} G_5 A^5 + \frac{21}{64} G_7 A^7 \right) \approx -0.22, \\ C_5(A) &\approx \left(\frac{1}{16} G_5 A^5 + \frac{7}{64} G_7 A^7 \right) \approx 0.019, \text{ and} \\ C_7(A) &\approx \left(\frac{1}{64} G_7 A^7 \right) \approx -0.00098. \end{aligned} \tag{85}$$

Of these, the third harmonic is clearly the strongest. The fifth harmonic is more than 20 dB lower than the third harmonic.

We identify the power in the desired signal as

$$P_0 = \frac{A^2}{2}. \tag{86}$$

We identify the power in the undesired third harmonic due to INL as

$$P_3 = \frac{\left(qC_3(A)\right)^2}{2}. \tag{87}$$

The relative spur power level is

$$\frac{P_3}{P_0} = \left(\frac{qC_3(A)}{A}\right)^2 \approx \left(\frac{0.22/256}{0.4}\right)^2 \approx 4.65\times10^{-6}. \tag{88}$$

This relative spur power level equates to –53 dBc.

So, for a sinusoidal INL with peak value of ½ LSB, and an input signal with $A = 0.4$, this generates a third harmonic at a level of –53 dBc. A simulation of this example is illustrated in Figure 4. The spur in fact is measured at –53 dBc as predicted.

For this example, the total INL distortion energy calculates to –46 dBc. This compares to the –53 dBc calculated above for the third harmonic. The difference is due to a strong fundamental harmonic component.

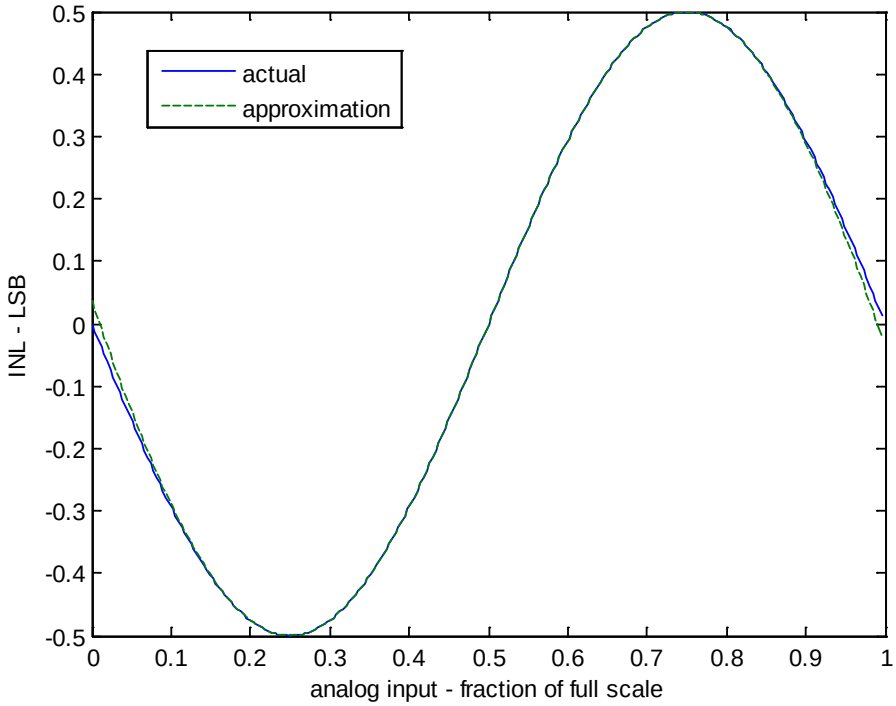

Figure 3. Example sinusoidal INL characteristic with approximation.

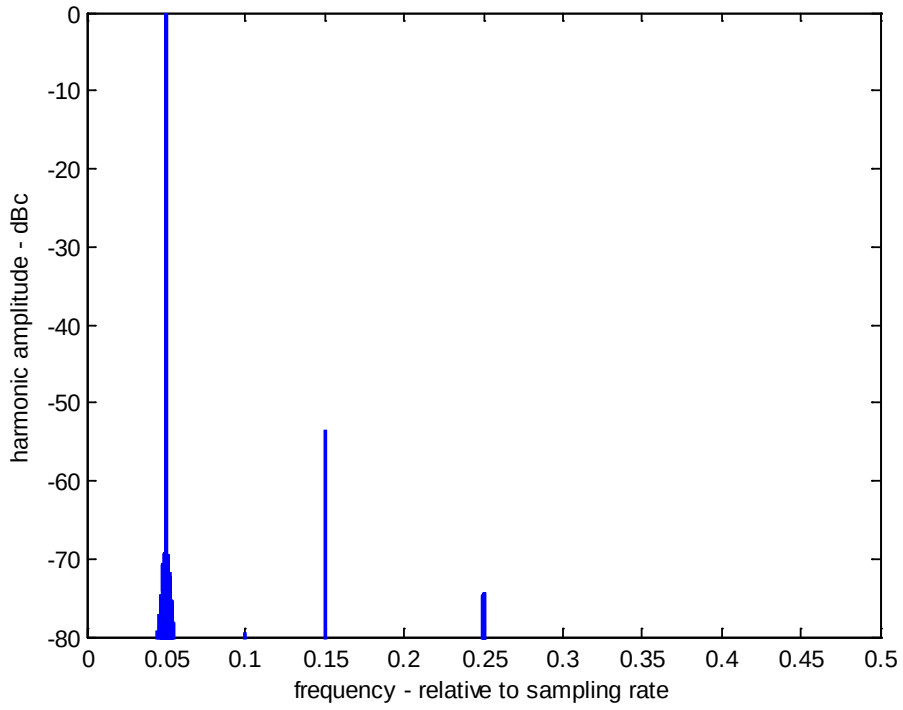

Figure 4. Spectrum of harmonic distortion.

2.3.3 Uniformly Distributed Random INL Function

Consider now an INL function that is made up of uniformly distributed random samples in the interval $[-1/2,1/2)$.

We reason that such an INL has relatively little or no low-order structure. What structure there is, is purely accidental owing to random chance. Consequently we would expect very low levels of low-order harmonics, and in fact generally low levels of all harmonics. However, random means random, which in fact does allow for accidentally occurring apparent low-order structure, which can allow for elevated harmonic content in some cases. Furthermore, this is in fact quite typical.

Furthermore yet, the randomness indicates large derivatives, which implies significance of higher-order harmonics.

One such example is illustrated in Figure 5. Superimposed on this INL characteristic is a 9^{th} order polynomial fit to the random values. The corresponding spectrum is shown in Figure 6. This particular example exhibits a measured peak harmonic spur at –57 dBc.

The spectrum of two other ensemble members of random INL functions are shown in Figure 7 and Figure 8.

For this example, the total INL distortion energy calculates to –48 dBc. However, in the example, this is spread amongst 10 distinct harmonics, suggesting that any one harmonic averages one tenth of the energy available. Consequently for uniform apportionment we would then expect –58 dBc harmonic levels. We also note that the quantization operation will itself induce some nearly random modulation that will further spread this energy slightly, reducing the average harmonic spur level even further. Then again, random nature will of course allow for some harmonic spurs to be above the mean level. We are of course interested in the peak harmonic spur level. Choosing an input signal at a different frequency to allow for more harmonics will indeed spread the distortion energy amongst more harmonics, but would also allow for more chances at a substantially higher than normal individual harmonic spur level. A reasonable guess at the peak harmonic spur level seems to be 10 dB below the INL distortion energy prediction. This rule-of-thumb approximation seems to hold over a large parameter space of signal amplitudes and signal frequencies. For our example parameters, this corresponds to an expected –58 dBc peak harmonic spur level. This compares to the –57 dBc measured above for the strongest harmonic component in Figure 6. The two subsequent random INL characteristic samples exhibit –59 dBc peak harmonic spurs.

We repeat here the subtle observation that the quantization noise itself tends to somewhat smear INL distortion energy. This suggests that additional noise, by whatever source, has the potential to smear the INL distortion energy even further, thereby reducing peak levels below those cited. Simulations validate this.

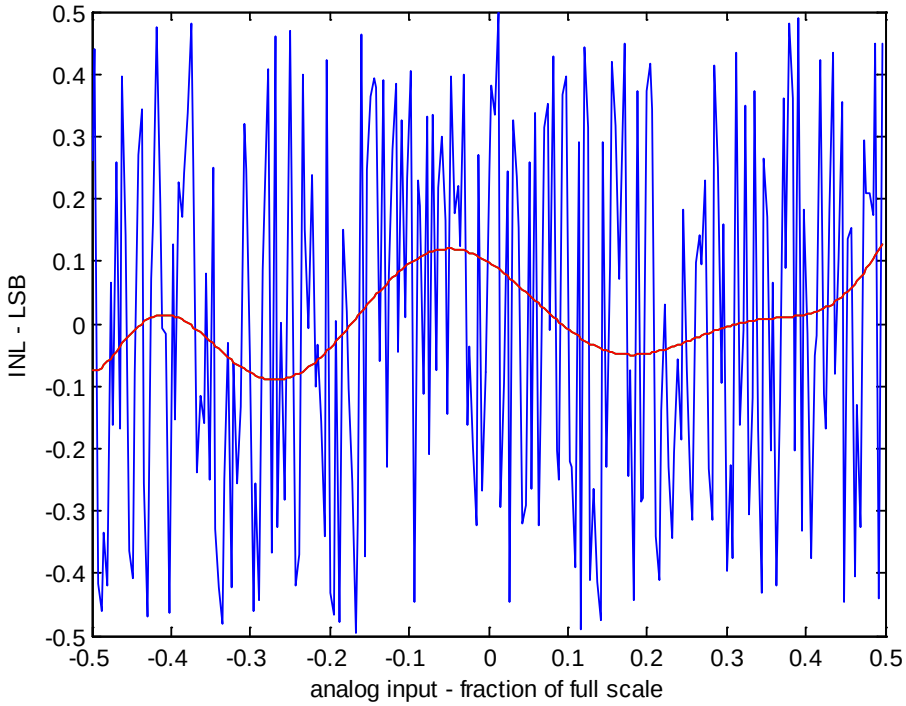

Figure 5. Example random INL characteristic.

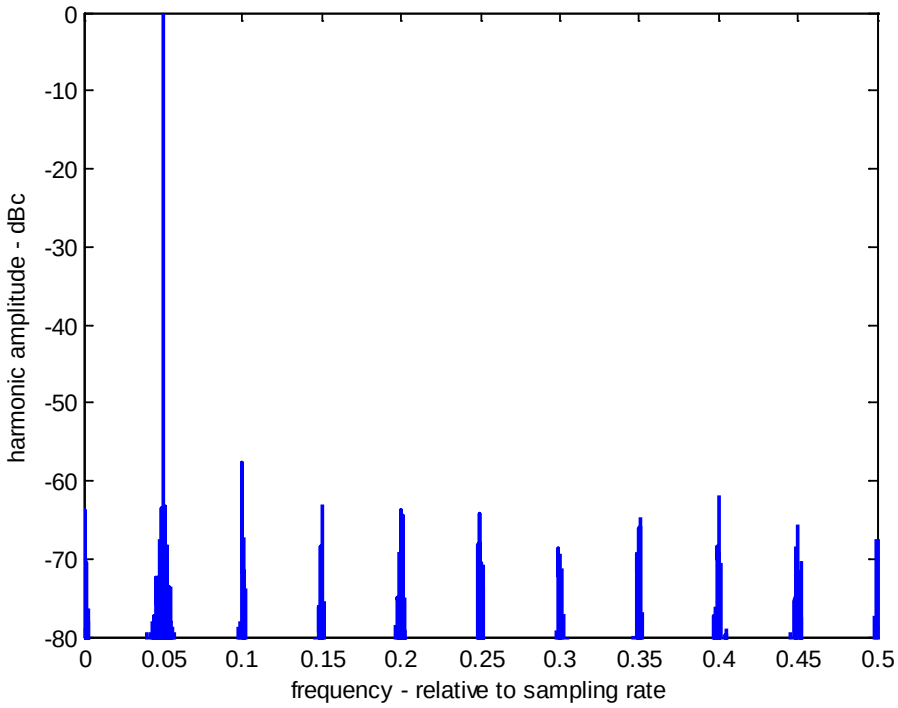

Figure 6. Spectrum of harmonic distortion.

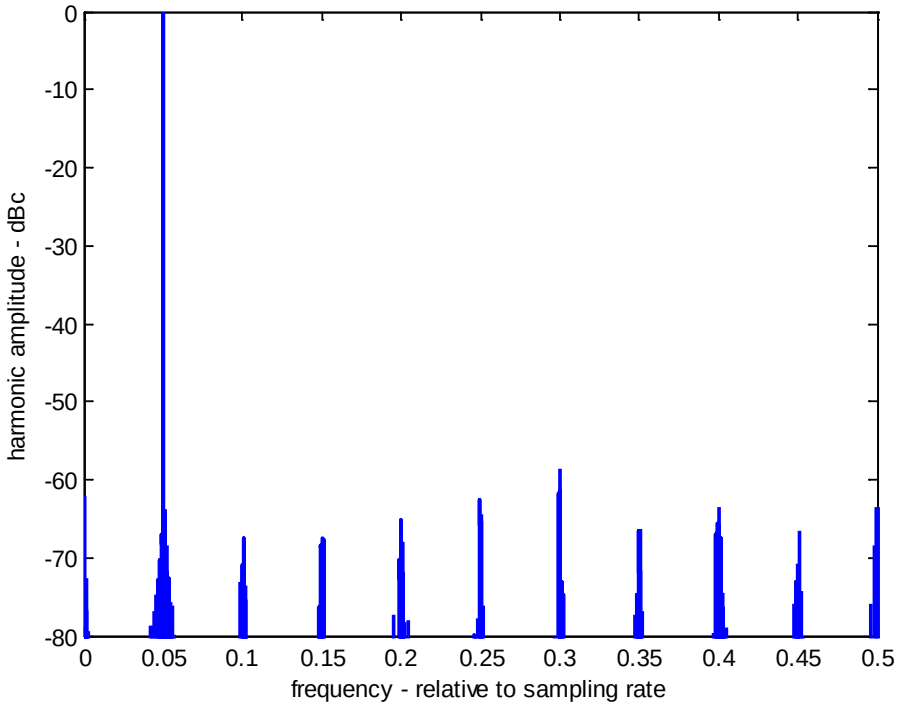

Figure 7. Spectrum of harmonic distortion.

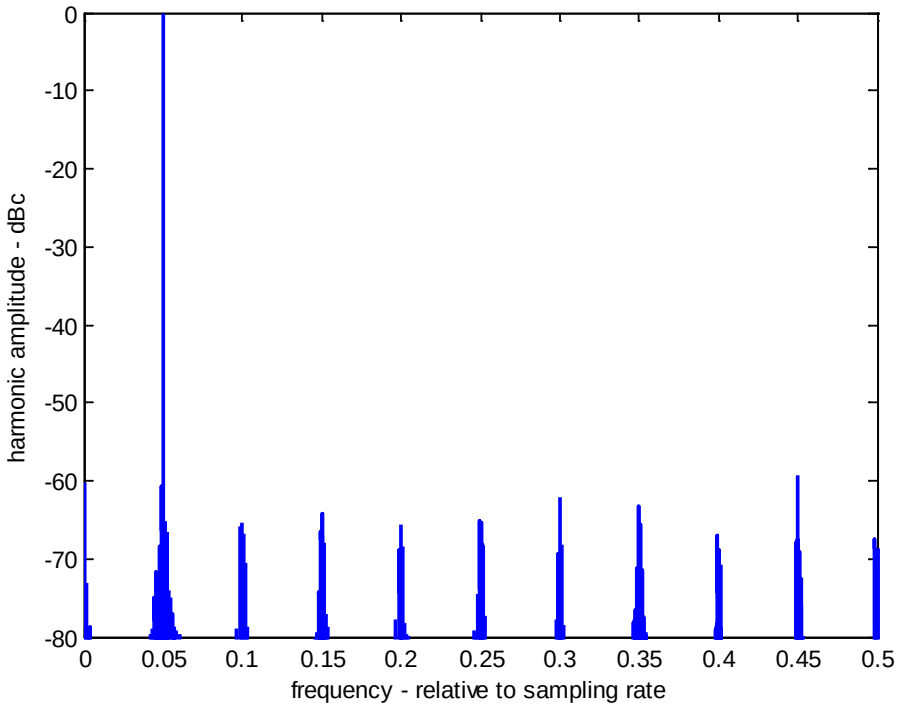

Figure 8. Spectrum of harmonic distortion.

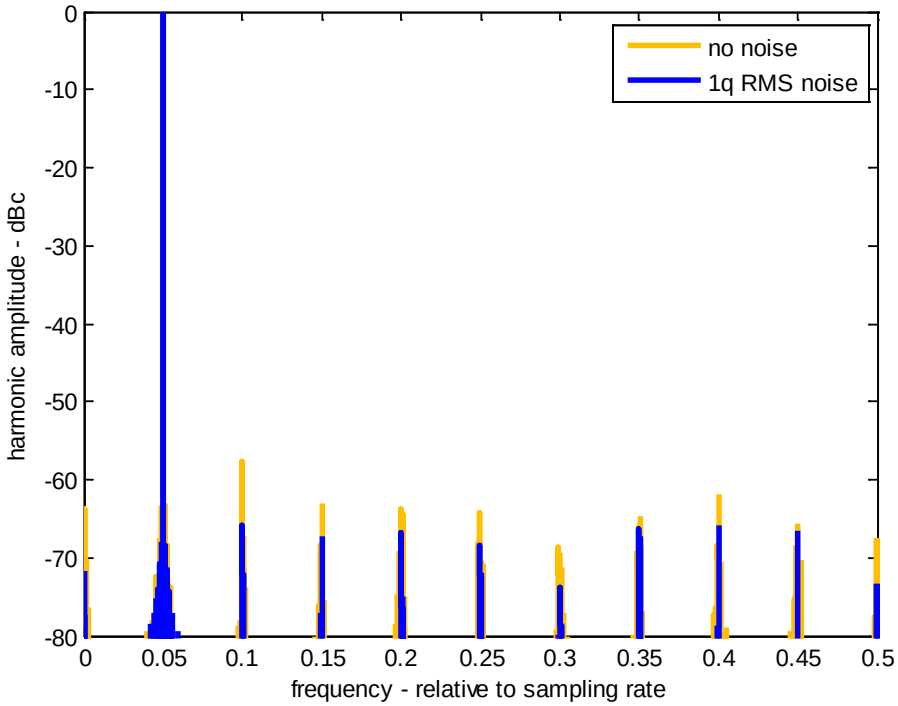

Figure 9. Spectrum of harmonic distortion with AWGN.

2.3.4 Uniformly Distributed Random INL Function with Added Input Noise

Consider again the INL function that is made up of uniformly distributed random samples in the interval $[-1/2,1/2)$. The signal is still 10,000 samples of a sinusoidal input with amplitude $A = 0.4$, but also with Additive White Gaussian Noise (AWGN) with an RMS level equal to the quantization step size *q*. To push down the noise floor, we will average 100 such processed vectors, with independent AWGN samples. This is simulated with results illustrated in Figure 9. This example uses the INL characteristic of Figure 5.

Note that in this example, peak harmonic spur levels have been reduced from –58 dBc to –65 dBc. While this and other simulations show that most harmonic spurs are improved (diminished) by the AWGN, not all spurs are always improved, and sometimes this means the largest spur is one that is not improved.

Larger amounts of AWGN tend to reduce the average level of harmonic spurs even more so, but do not necessarily guarantee a substantial reduction of any one spur, including perhaps the largest one. Figure 10 illustrates the same conditions as Figure 9, except that the AWGN RMS level has been increased to 4 times the quantization level, and the number of averaged vectors to push down the final noise floor has been increased to 400. A second simulation with different noise, albeit the same statistics, is illustrated in Figure 11.

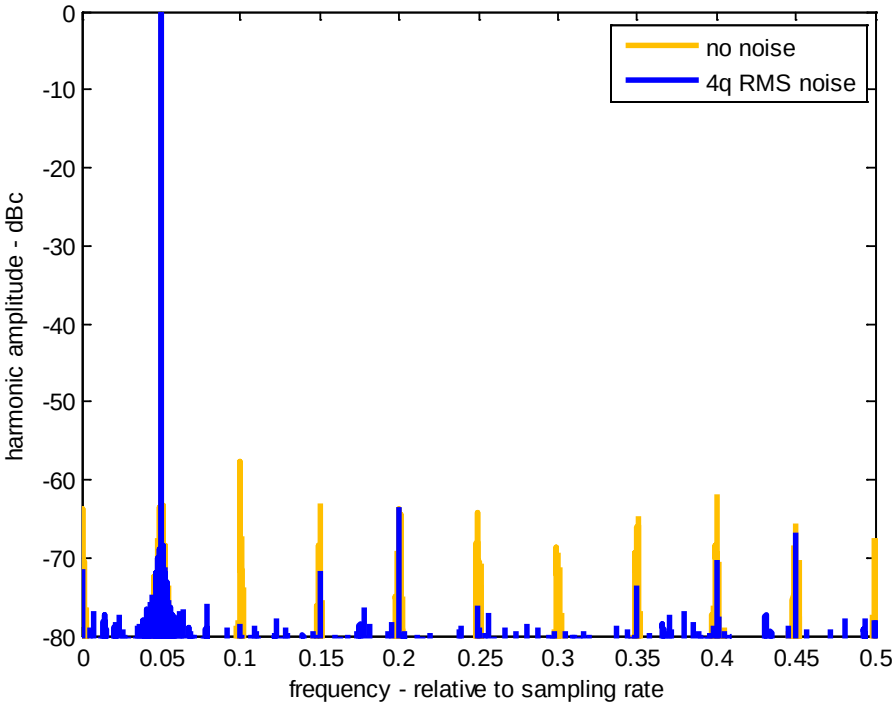

Figure 10. Spectrum of harmonic distortion with AWGN.

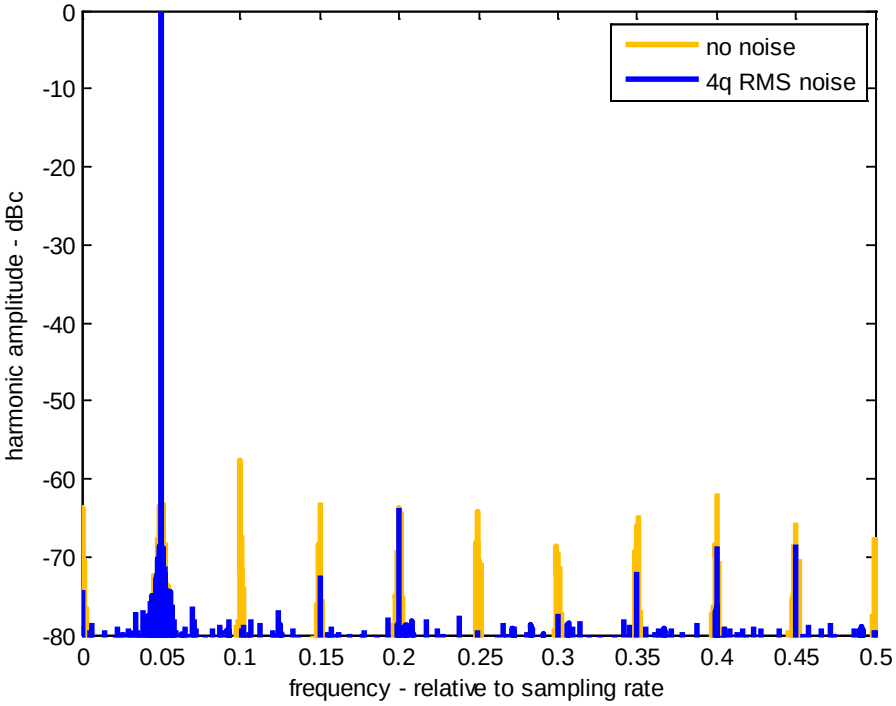

Figure 11. Spectrum of harmonic distortion with AWGN.

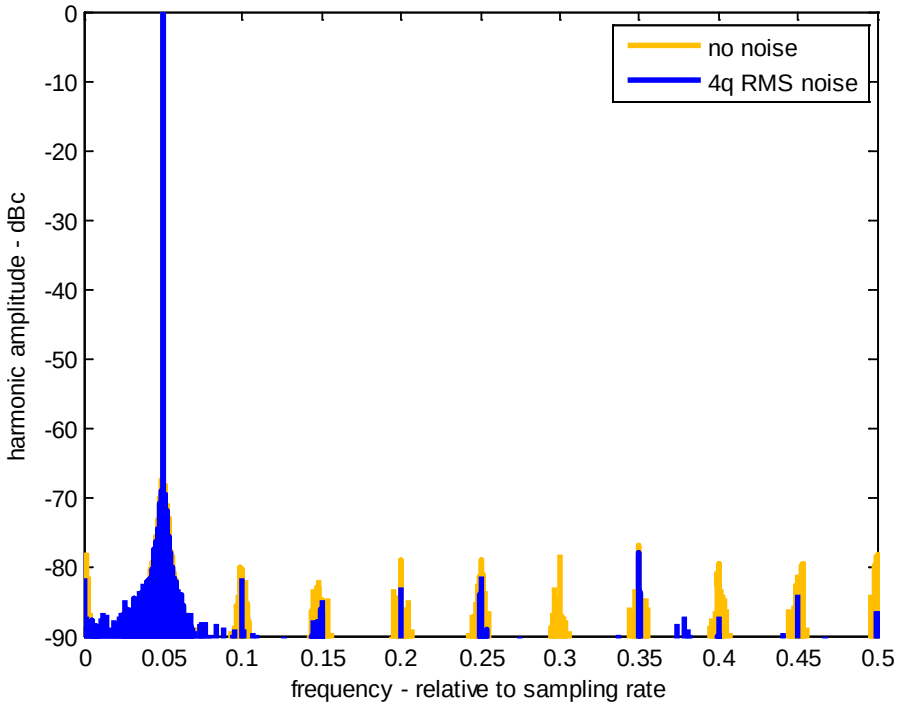

Figure 12. Spectrum of harmonic distortion with AWGN, 10-bit ADC.

If we increase the number of ADC bits to 10, with AWGN at 4 times the quantization level, then we might achieve the harmonic spur levels illustrated in Figure 12. This example exemplifies a peak harmonic spur content at –79 dBc.

2.4 Digital Down-Conversion Issues

The harmonic spurs caused by INL are generated right at the analog to digital conversion process. Consequently, unlike the main target signal, harmonic spurs are not affected at all by any analog filters earlier in the signal path. These harmonic spurs may manifest at any frequency in the raw ADC samples' frequency space. Furthermore, harmonic spurs may manifest at frequencies well beyond the ADC sampling frequency, and then be aliased down to frequencies anywhere below the ADC sampling frequency.

At the ADC component output, the raw data bandwidth is equal to the sampling frequency. The data is real-valued, so the data spectrum is unique over only half the data bandwidth.

As described in earlier sections of this report, for digital down-conversion, the data spectrum of interest rides on an IF carrier that is ¼ the sampling frequency, or $f_s/4$. Subsequent to the conversion process, the data is shifted in frequency to baseband and filtered, in the process becoming complex-valued, or I/Q data. This is also known as digital demodulation followed by filtering. The filter is known as the demodulation filter, defined as $h_{demfil}(n)$ above.

The key point here is that the demodulation filter has a passband width that is generally somewhat less than $f_s/4$. Subsequent filtering in the DRX might reduce the passband even further. In any case, not all harmonic spurs will make it through these filters. At the very least some will be substantially attenuated by the digital filters' stopband performance.

We illustrate this with the following example, where we will presume

$$\begin{aligned} &f_s = 1 \text{ GHz}, \\ &B_{demfil} = 220 \text{ MHz} = \text{two-sided bandwidth of } h_{demfil}(n). \end{aligned} \tag{89}$$

We shall presume that the target response is a sinusoid with offset frequency

$$f_d = -100 \text{ MHz}. \tag{90}$$

This collection of parameters, in addition to the INL specification of Figure 5, is illustrated in Figure 13. The demodulator filter's effective passband transmogrified to the IF center frequency is high-lighted in pink, with the relevant signal and harmonic spurs in red. A detailed listing of the harmonic content, and how they alias, is summarized in Table 1.

For this contrived one-dimensional example, harmonics of order 21 and higher will alias on top of lower order harmonics. This is not true in general.

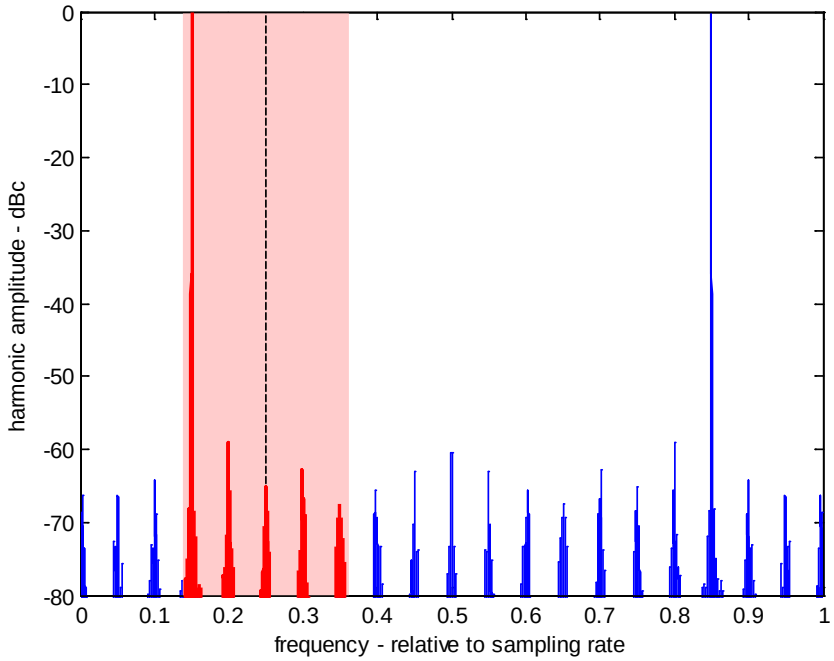

Figure 13.

Table 1. Harmonic location of spurs in Figure 13.

harmonic number	***frequency MHz***	***alias MHz***
1	150	**150**
2	300	**300**
3	450	450
4	600	600
5	750	750
6	900	900
7	1050	50
8	1200	**200**
9	1350	**350**
10	1500	500
11	1650	650
12	1800	800
13	1950	950
14	2100	100
15	2250	**250**
16	2400	400
17	2550	550
18	2700	700
19	2850	850
20	3000	0
21	*3150*	*150*

Note that not all harmonic spurs are in the filter's effective passband. Those outside the effective passband will be attenuated by the demodulator filter. A subsequent data decimation operation may then cause their attenuated versions to alias into the effective passband. Nevertheless, the most important harmonic spurs are those within the filter's effective passband. These are the 'in-band' spurs.

We also note that the relevant in-band spurs are not necessarily those of low harmonic order. We observe that the order of appearance of the various harmonic spurs within the effective passband from low frequency to high is as follows:

1. Fundamental, or main target signal
2. 8^{th} harmonic spur
3. 15^{th} harmonic spur
4. 2^{nd} harmonic spur
5. 9^{th} harmonic spur

The strongest harmonic spur in this particular example is the 8^{th} harmonic, and it is 'in-band'.

As a final note, in the case of additional filtering after the demodulation filter to reduce the passband even further, such a filter may attenuate the fundamental signal, and yet still pass the appropriate harmonic. This means that in a range-Doppler map, a target outside the scene of interest can still generate harmonic spur content within the scene.

Out of Band Dither

It is generally desired to allow some degree of AWGN in the ADC input signal to whiten the quantization noise. This is often termed "dither". A desired level for the dither is an RMS level equal to the quantization step size *q*.

Digital down conversion generally presumes that the signal of interest occupies a bandwidth less than one fourth of the sampling frequency. Consequently there is a readily identified out-of-band spectral region presented to the ADC. Furthermore, this out-of-band spectral region is filtered away later anyway. This presents an opportunity to apply an appropriate noise dither signal that is advantageously limited to this out-of-band spectral region. The band-limited noise thereby provides its dither function, but does not itself add to the noise floor of the signal spectrum.[5]

“Nothing and no one is perfect.
It just takes a good eye to find those hidden imperfections.”
— Daphne Delacroix

3 INL and GMTI

We examine here the impact of INL spurs on a typical GMTI mode. Basic exo-clutter GMTI performance is discussed in an earlier report.[6] Basic performance parameters for DMTI are discussed in a paper by Doerry, et al.[7]

3.1 Typical GMTI Processing in a Nutshell

We shall presume a typical GMTI mode that uses stretch processing, whereby the Linear FM (LFM) chirp echoes are de-chirped prior to sampling. Target energy then manifests at a constant frequency. Range resolution is generally coarse with respect to target dimensions.

A typical raw data set for typical GMTI mode might include 1024 fast-time samples for each of 256 pulses. Fewer fast-time samples might be collected at nearer ranges. The actual number of pulses integrated will depend on radar Pulse-Repetition Frequency (PRF) and desired integration time, or Coherent Processing Interval (CPI).

A 2D-DFT on the data from a collection of pulses causes the target to manifest as a point response in the range-Doppler map.

A CFAR algorithm then compares each range-Doppler pixel (in the exo-clutter region) to local noise statistics, and declares a 'detection' when a magnitude threshold is exceeded. These detections might be further filtered by subsequent detection logic involving multiple CPIs. This is often called Multiple Observation Signal Processing (MOSP).

A threshold for initial detection may include criteria for Signal to Noise Ratio (SNR) and Radar Cross Section (RCS). Example detection criteria are $\mathrm{SNR} \geq 20$ dB, and $\mathrm{RCS} \geq 0$ dBsm for vehicles, and perhaps $\mathrm{RCS} \geq -10$ dBsm for dismounts.

The effect of INL distortion is to introduce other frequency components that have the same signature as legitimate targets. Consequently, INL distortion produces non-existent phantom target signatures. If a phantom target signature exceeds the detection criteria, then it is declared a detection. This generates in fact a False Alarm detection.

If the phantom target signature is not declared a detection, then it still raises the noise floor in the range-Doppler map, thereby reducing the detection probability for other targets. That is, it reduces the Probability of Detection. This is especially true if the phantom target signature contains significant energy with respect to the expected noise floor.

Phantom target signatures below the noise floor are generally considered inconsequential to the detection process.

3.2 Some Basic Truths

The following basic truths will direct the subsequent analysis.

- INL spur levels depend on signal levels in a nonlinear fashion.
- INL spurs should be low enough to not generate False Alarms. They should also ideally not contribute to degradation of the Probability of Detection.
- Spur levels at or below the noise level in the range-Doppler map will be inconsequential to GMTI operation.
- Spur levels sufficiently below the minimum RCS level will be inconsequential to GMTI operation. The amount below the minimum RCS level corresponds to the minimum SNR level required for detection.
- Large RCS targets need to exhibit lower relative INL spurs than do smaller RCS targets. Consequently, spur energy level relative to signal energy (e.g. with units dBc) is signal level dependent. This falls out of an RCS threshold criterion.

3.3 Basic GMTI Performance Parameters

We address now some basic GMTI/DMTI performance parameters used in subsequent calculations. Many of the parameters discussed below are justified in the paper by Doerry, et al. [7]

3.3.1 Maximum Target RCS of Interest

The maximum target RCS of interest is more properly termed the "maximum target scene RCS allowable for which the radar still needs to operate properly." That is to say that this is not necessarily the RCS of a land vehicle, but could be a bright clutter discrete in the scene. We acknowledge that even if a clutter discrete is in the endo-clutter region of Doppler, its harmonic may in fact appear in the exo-clutter region. Consequently, we are interested in the maximum expected values for clutter discretes. Evidence suggests that a clutter discrete will exceed 45 dBsm approximately once per square mile. We shall consider this level as an upper limit, beyond for which we will accept the occasional false alarm.

3.3.2 Minimum Target RCS of Interest

GMTI target RCS will fluctuate with aspect viewing angle. A typical fluctuation characteristic is identified as Swerling I. To guarantee a detection probability of 90% or better, just due to target fluctuations alone, the RCS threshold needs to be 10 dB or more below the average target RCS level. Since a common average RCS specification is 10 dBsm for vehicles, this implies a minimum target RCS for detection of 0 dBsm or less. Reducing this will increase the Probability of Detection. Note that smaller targets, such as dismounts, will require even lower minimum threshold RCS, perhaps –10 dBsm or so.

3.3.3 Minimum SNR required for Detection

The Probability of False Alarm, or the False Alarm Rate (FAR), will depend on the threshold SNR for detection. Typical numbers for this range from 13 dB to 20 dB. A typical FAR spec is perhaps 0.1 Hz. This will tend to require a minimum SNR more towards the higher end of the typical range. The exact number will depend on other GMTI parameters such as area coverage rate, PRF, range resolution, etc. Reducing the SNR threshold will increase the FAR.

Note that clutter cancellation techniques attenuate clutter discretes, but will not necessarily eliminate them. Even moving targets will be attenuated somewhat, especially slow-moving targets.

3.3.4 Signal Processing Gain

A typical CPI for GMTI is perhaps 256 pulses with 1024 samples per pulse. The theoretical limit for this is 54 dB of coherent processing gain. i.e. gain in the SNR. Fairly substantial sidelobe suppression will reduce the achievable SNR gain by perhaps 4 dB or so. Fewer samples per pulse will reduce the coherent gain proportionately. Of course, more pulses will increase this again.

3.3.5 Summary

For subsequent development, we identify the parameters

$\sigma_{\max}$ = maximum target RCS of interest [3.16×10^4 or 45 dBsm],
$\sigma_{\min}$ = minimum target RCS of interest [0.1 or –10 dBsm],
$\eta_{img,\min}$ = minimum SNR required for detection [10^2 or 20 dB],
G_{sp} = signal processing coherent SNR gain after the ADC [10^5 or 50 dB]. (91)

We note that $\sigma_{\max}$ is based on expected clutter discretes. We acknowledge that large vehicles, especially maritime vessels, may often exceed this.

3.4 INL Spur Levels and GMTI Performance

The maximum input target signal power at the ADC is limited to

$$P_{ADC,\max} = \frac{\left(q2^{b-1}\right)^2}{2} = q^2 2^{2b-3}. \quad (92)$$

The input target signal level at the ADC is bounded by

$$P_0 \le P_{ADC,\max}. \quad (93)$$

Recall that the input target signal power is

$$P_0 = \frac{A^2}{2}. \tag{94}$$

This target will generate an INL spur at some level

P_{spur} = spur power generated by ADC INL for target sinusoidal input signal. (95)

We set the system noise level ADC input at some level with respect to the quantization step size as

$$N_{ADC} = G_N q^2, \tag{96}$$

where

G_N = the amount of system noise power in excess of 1 LSB RMS. (97)

We generally operate such that we have more than 1 LSB RMS of noise, implying

$$G_N \geq 1. \tag{98}$$

The SNR at the ADC input is then given by

$$\eta_{ADC} = \frac{P_0}{N_{ADC}} = \frac{A^2}{2G_N q^2}. \tag{99}$$

Note that the ADC input SNR is limited to

$$\eta_{ADC} \leq \frac{P_{ADC,\max}}{G_N q^2} = \frac{2^{2b-3}}{G_N}. \tag{100}$$

The maximum ADC input SNR occurs when $G_N = 1$, and for an 8-bit ADC equates to a net 39 dB. We will assume this going forward.

The system noise manifests in the range-Doppler image with power

$$N_{img} = \frac{N_{ADC}}{G_{sp}}. \tag{101}$$

3.4.1 False Alarms

For the spur level to be guaranteed to be less than the detection threshold to generate a False Alarm, we require

$$\frac{P_{spur}}{P_0} \le \left(\frac{\sigma_{\min}}{\sigma_{\max}} \right). \tag{102}$$

For typical values, this amounts to –55 dBc. This means that harmonic spur levels below –55 dBc will not generate excessive false alarms from clutter discretes due to the RCS threshold criterion. In addition, for the spur level to be adequately low with respect to the range-Doppler image noise level so as to not generate False Alarms, we require

$$P_{spur} \le \eta_{img,\min} N_{img} \,. \tag{103}$$

Consequently, the relative spur level is limited to

$$\frac{P_{spur}}{P_0} \le \frac{\eta_{img,\min}}{\eta_{ADC} G_{sp}} \,. \tag{104}$$

For a maximum sinusoid input to the ADC, and other typical values, this amounts to about –69 dBc. Note that this does not depend on $\sigma_{\max}$. This means that harmonic spurs below –69 dBc are guaranteed to not generate false alarms due to the SNR criterion, for all signal levels including the maximum that the ADC can pass without clipping. However, the harmonic spur criteria will change with signal level, and not guaranteed to do so in a linear fashion. The requirement for not excessively generating False Alarms then becomes meeting either

$$\frac{P_{spur}}{P_0} \le \left(\frac{\sigma_{\min}}{\sigma_{\max}} \right) \quad \text{or} \quad \frac{P_{spur}}{P_0} \le \frac{\eta_{img,\min}}{\eta_{ADC} G_{sp}} \,. \tag{105}$$

Either of these criteria met will be adequate.

We reiterate that the numbers cited above are for the typical radar parameters given. The limits as a function of *A* are plotted in Figure 14. Note that for large signal levels the RCS criterion is sufficient, but for smaller signal levels the SNR criterion allows some relaxation.

3.4.2 Probability of Detection

For the spur level to be guaranteed to not adversely affect Probability of Detection, we require the spur to be in the noise, or

$$\frac{P_{spur}}{P_0} \le \left(\frac{\sigma_{\min}}{\eta_{img,\min}\sigma_{\max}} \right). \tag{106}$$

For typical GMTI/DMTI values, this amounts to −75 dBc. This means that harmonic spur levels below −75 dBc will not excessively affect the probability of detection due to the RCS criterion for clutter discretes.

For the spur level to be at or below the range-Doppler image noise level to not adversely affect Probability of Detection, we require

$$P_{spur} \le N_{img}\,. \tag{107}$$

Consequently, the relative spur level is limited to

$$\frac{P_{spur}}{P_0} \le \frac{1}{\eta_{ADC} G_{sp}}\,. \tag{108}$$

For a maximum sinusoid input to the ADC, and other typical values, this amounts to about −89 dBc. Note that this does not depend on $\sigma_{\max}$. This means that harmonic spurs below −89 dBc are guaranteed to not adversely affect the probability of detection due to the SNR criterion, for all signal levels including the maximum that the ADC can pass without clipping. However, the harmonic spur criteria will change with signal level, and not be guaranteed to do so in a linear fashion.

The requirement for not excessively degrading Probability of Detection then becomes meeting either

$$\frac{P_{spur}}{P_0} \le \left(\frac{\sigma_{\min}}{\eta_{img,\min}\sigma_{\max}} \right) \quad \text{or} \quad \frac{P_{spur}}{P_0} \le \frac{1}{\eta_{ADC} G_{sp}}\,. \tag{109}$$

Either of these criteria met will be adequate. Note that this is just the criteria for False Alarms scaled by the inverse of the required SNR, namely $\left(\eta_{img,\min}\right)^{-1}$.

We reiterate that the numbers cited above are for the typical radar parameters given. The limits as a function of amplitude *A* are plotted in Figure 15. Note that for large signal levels the RCS criterion is sufficient, but for smaller signal levels the SNR criterion allows some relaxation.

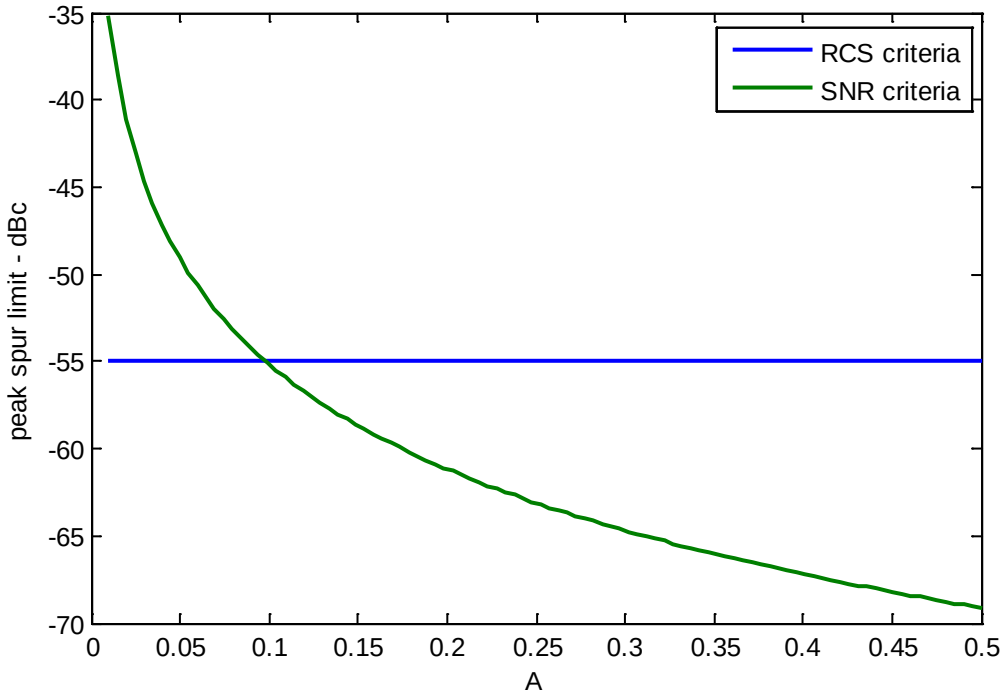

Figure 14. Harmonic spur limits to prevent false alarms. This assumes typical GMTI/DMTI parameters with 8-bit ADC.

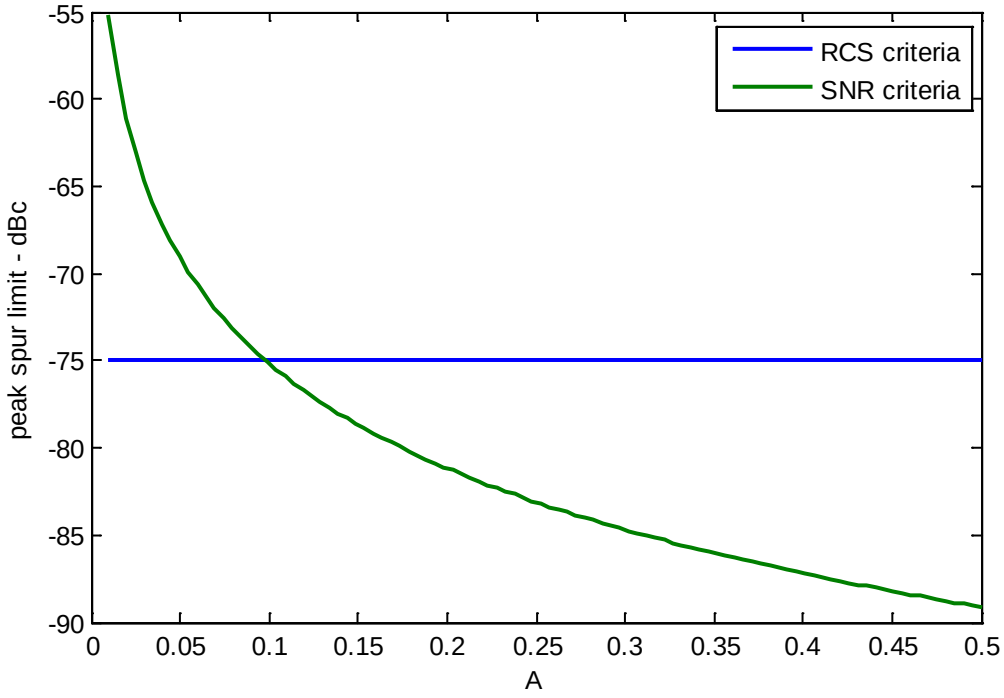

Figure 15. Harmonic spur limits to not impact probability of detection. This assumes typical GMTI/DMTI parameters with 8-bit ADC.

3.4.3 Some Comments

We now offer some additional notes.

- The examples cited above presume typical GMTI/DMTI parameters as given.

- Modes like DMTI will need exceptionally 'clean' harmonic content, because of the desire to detect smaller RCS targets. Quite simply, Smaller RCS detection thresholds mean that spurs are more likely to cause false alarms.

- INL will also cause a DC spur. This spur will be attenuated by the demodulation filter, but some residual DC will likely exist to alias to mid-range in a range-Doppler map. The large coherent processing gain of SAR will likely allow this to manifest in the SAR image. Since this DC component is scene clutter dependent, any DC-cancellation techniques may find it difficult to 'keep up' with the changing DC value from image to image.

- The harmonic spur levels in a range-Doppler map are a highly nonlinear and non-monotonic function of signal amplitude, frequency, and background noise. Furthermore, variations in INL characteristics from one ADC to another, even of the same type, will generate large differences in any particular harmonic spur level.

3.5 Some Comments on the Range-Doppler Map

The harmonic spur analysis heretofore has generally been exemplified with one-dimensional plots. However, as indicated above, an intermediate product for GMTI processing is a two-dimensional range-Doppler map.

In such a range-Doppler map, with sufficiently high radar PRF, stationary clutter manifests itself generally as a narrow band of clutter echoes generally extending across all ranges. This clutter band, even if centered at zero Doppler with respect to the center reference range, need not be centered at zero Doppler at all ranges. That is, the Doppler band need not be vertical in a range-Doppler map. This is explored in detail in an earlier report.[8] Furthermore, while the clutter band may be narrow, it does indeed have some width. In any case, we may expect even stationary clutter to have a significant non-zero Doppler at times. This is precisely the phenomenon exploited by SAR.

The bottom line is that harmonic spurs may be shifted in range as well as Doppler. Consequently, clutter discretes can manifest anywhere in the range-Doppler map. Furthermore, different harmonic spurs may exhibit any combination of same or different range or Doppler.

4 INL Measures of Example ADC Components

We now examine some INL characteristics from a sampling of commercial ADCs, and analyze their nature to evaluate expected performance in GMTI applications.

4.1 ADC Component #1

The first ADC is an 8-bit device with INL characteristic from its data sheet reproduced in Figure 16.

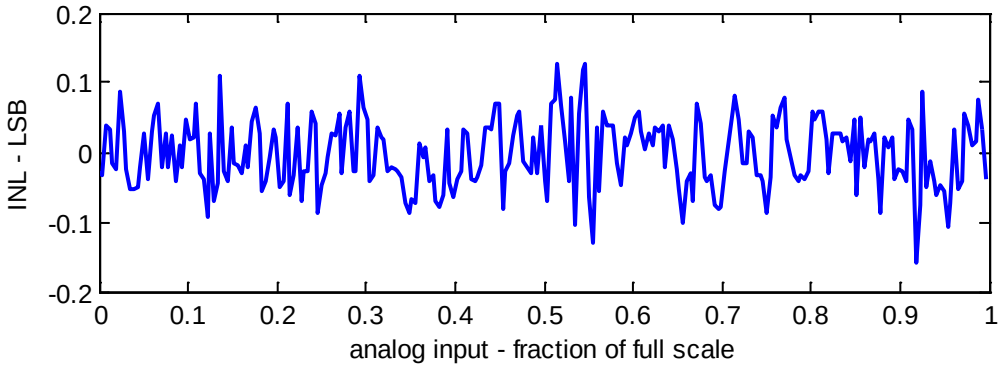

Figure 16. INL vs. output code for ADC Component #1.

Anecdotal evidence indicates substantial satisfaction with its performance in GMTI applications. Consequently, it has become the de facto standard by which other ADCs are being judged. The digitized INL characteristic was then subjected to simulations for harmonic spur analysis. We illustrate two examples using typical GMTI parameters.

The first example collects and averages 256 vectors of 1024 samples each of a sinusoidal input with amplitude $A = 0.4$, but also without and with AWGN with an RMS level equal to the quantization step size *q*, is shown in Figure 17. Peak harmonic spurs are –74 dBc without noise, and –74 dBc with noise. This is adequate to not cause excessive false alarms, but may degrade probability of detection slightly.

The second example collects averages 256 vectors of 1024 samples each of a sinusoidal input but with amplitude $A = 0.1$, also with AWGN with an RMS level equal to the quantization step size *q*, is shown in Figure 18. Peak harmonic spurs are –62 dBc. This is well below the corresponding threshold of –55 dBc to cause excessive false alarms. In this case, INL will not cause a false alarm at this signal level, which is independent of RCS.

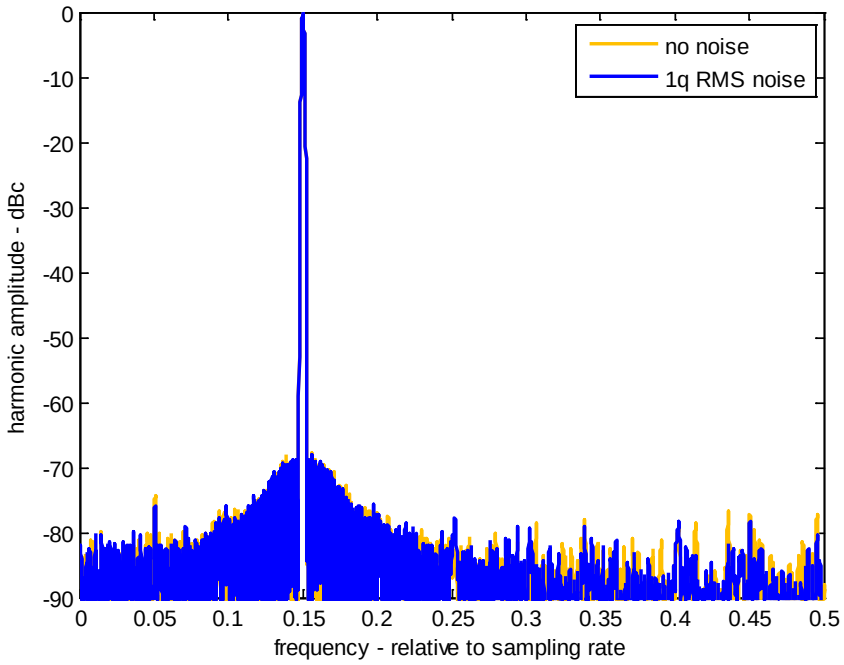

Figure 17. Spectrum of harmonic distortion produced by ADC Component #1 INL characteristic with and without AWGN. Signal level at *A*=0.4.

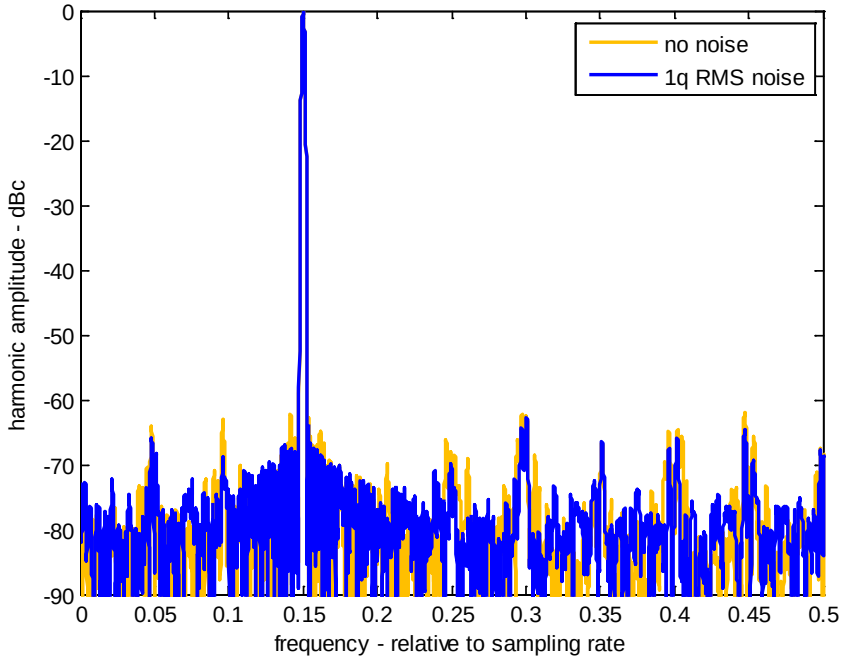

Figure 18. Spectrum of harmonic distortion produced by ADC Component #1 INL characteristic with and without AWGN. Signal level at *A*=0.1.

4.2 ADC Component #2

The second ADC is also an 8-bit device with INL characteristic from its data sheet reproduced in Figure 19. Note the low-order structure.

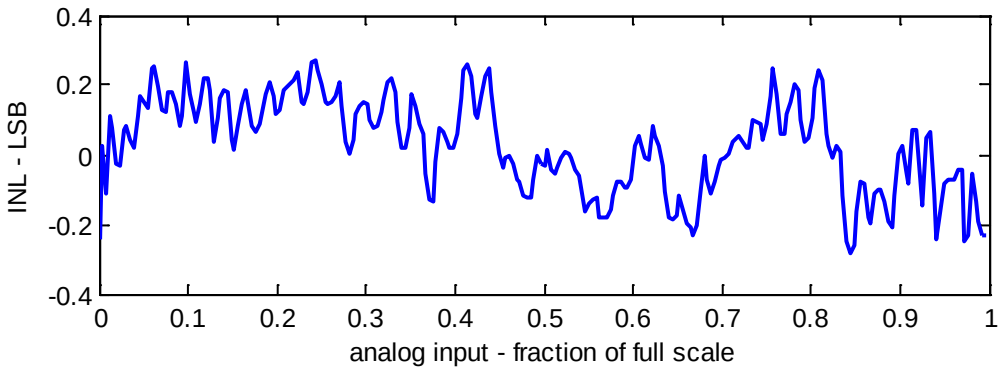

Figure 19. INL vs. output code for ADC Component #2.

This digitized INL characteristic was subjected to simulations for harmonic spur analysis. We illustrate two examples using typical GMTI parameters.

The first example collects averages 256 vectors of 1024 samples each of a sinusoidal input with amplitude $A = 0.4$, but also without and with AWGN with an RMS level equal to the quantization step size *q*, is shown in Figure 20. Peak harmonic spurs are –64 dBc. This is adequate to not cause excessive false alarms, but will degrade probability of detection.

The second example collects averages 256 vectors of 1024 samples each of a sinusoidal input but with amplitude $A = 0.1$, also with AWGN dither with an RMS level equal to the quantization step size *q*, is shown in Figure 21. Peak harmonic spurs are –52 dBc. This is above the corresponding threshold of –55 dBc to cause a false alarm. In this case, INL will cause a false alarm at this signal level, if this signal level corresponds to a +45 dBsm clutter discrete, and –10 dBsm targets are desired to be detected. This is judged to be unsatisfactory performance.

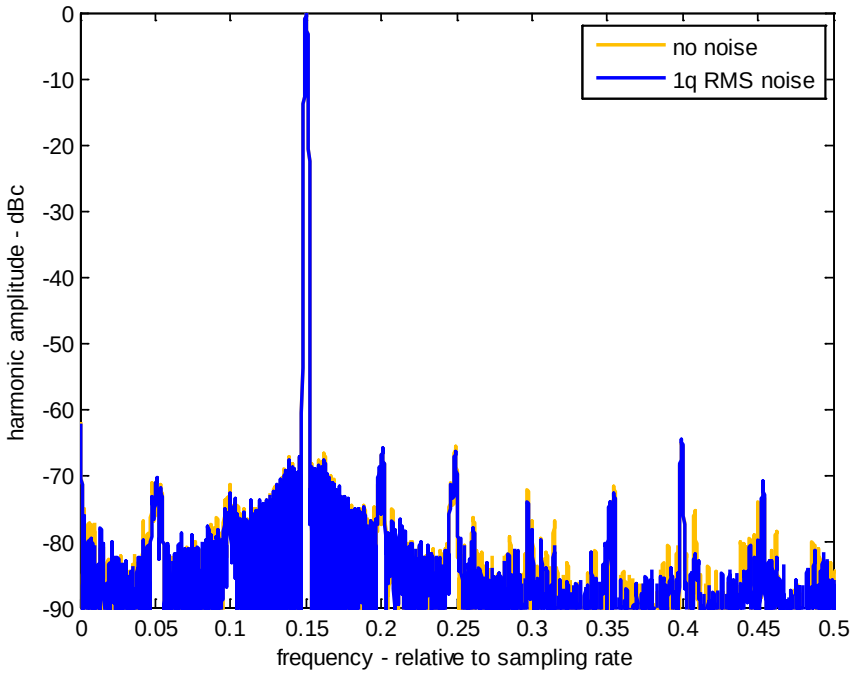

Figure 20. Spectrum of harmonic distortion produced by ADC Component #2 INL characteristic with and without AWGN. Signal level at *A*=0.4.

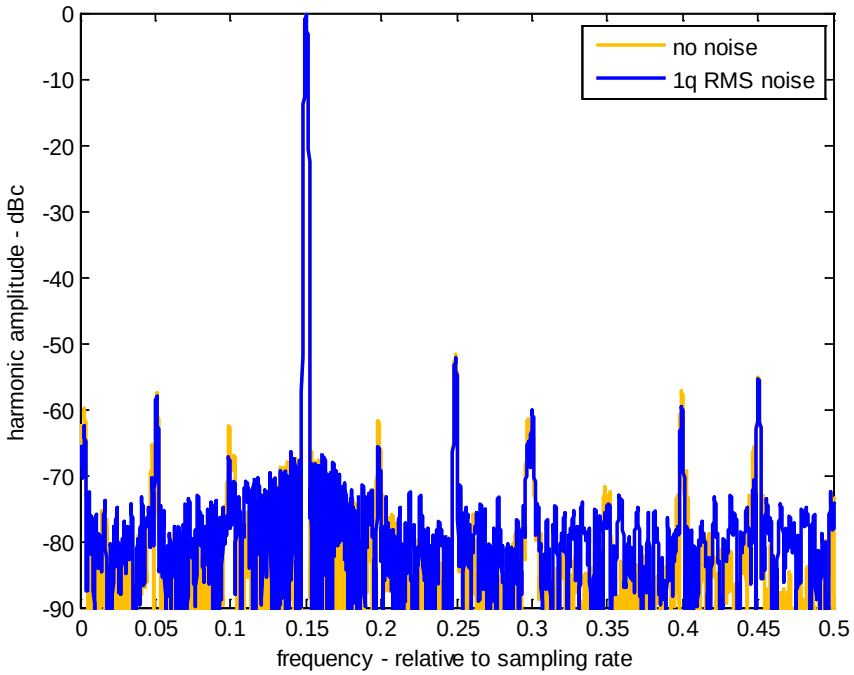

Figure 21. Spectrum of harmonic distortion produced by ADC Component #2 INL characteristic with and without AWGN. Signal level at *A*=0.1.

4.3 ADC Component #3

The third ADC is a 10-bit device with INL characteristic from its data sheet reproduced in Figure 22.

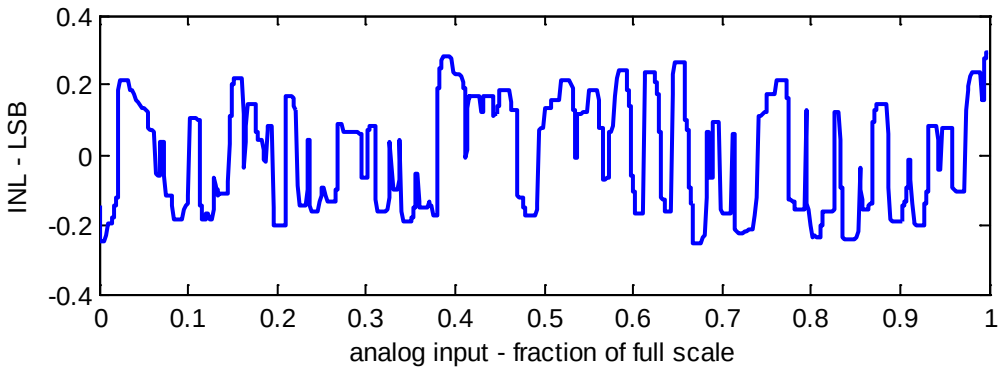

Figure 22. INL vs. output code for ADC Component #3.

The digitized INL characteristic was subjected to simulations for harmonic spur analysis. We illustrate two examples using typical GMTI parameters.

The first example collects averages 256 vectors of 1024 samples each of a sinusoidal input with amplitude $A = 0.4$, but also without and with AWGN dither with an RMS level equal to 4 times the quantization step size q, is shown in Figure 23. Peak harmonic spurs are –74 dBc without noise, and –75 dBc with noise. This is adequate to not cause excessive false alarms, but may degrade probability of detection slightly.

The second example collects averages 256 vectors of 1024 samples each of a sinusoidal input but with amplitude $A = 0.1$, also with AWGN dither with an RMS level equal to 4 times the quantization step size q, is shown in Figure 24. Peak harmonic spurs are –61 dBc, the DC term notwithstanding. This is well below the corresponding threshold of –55 dBc to cause a false alarm. In this case, INL will not cause a false alarm at this signal level if it corresponds to a +45 dBsm clutter discrete with a detection threshold of –10 dBsm.

This ADC is therefore roughly equivalent to the ADC Component #1 INL performance.

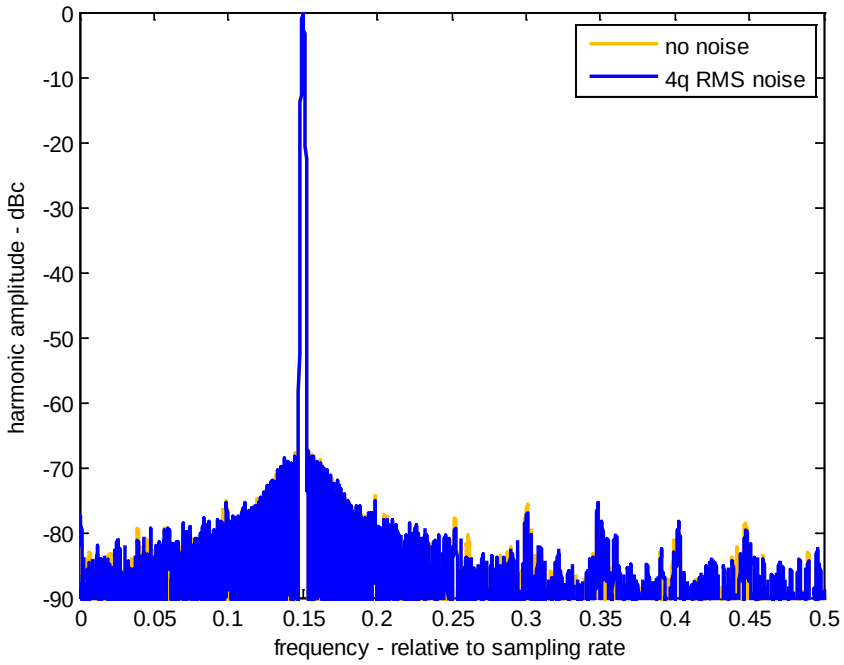

Figure 23. Spectrum of harmonic distortion produced by ADC Component #3 INL characteristic with and without AWGN. Signal level at *A*=0.4.

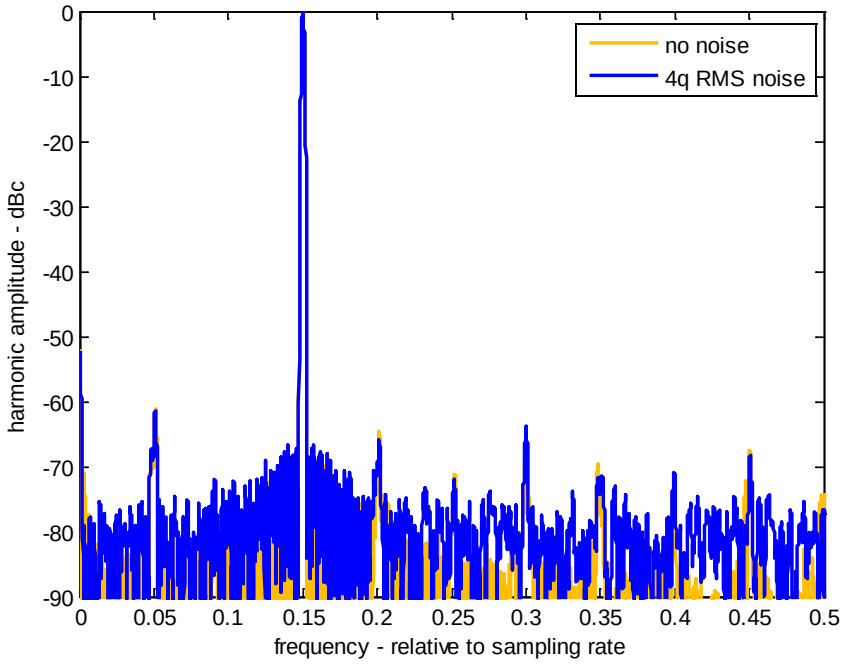

Figure 24. Spectrum of harmonic distortion produced by ADC Component #3 INL characteristic with and without AWGN. Signal level at *A*=0.1.

5 Mitigation Techniques

Mitigation techniques for unwanted spurious energy are generally implemented with the following order of precedence.

1. Reduce or eliminate the spurious energy,
2. Move the spurious energy to unwanted signal space,
3. Smear the spurious energy to reduce its coherence and peak value,
4. Image post-processing.

We examine these in turn, albeit in a very cursory manner. We do this by way of examples. Common parameters for all examples in this section include

8-bit ADC with INL characteristic of Figure 19.

Input signal with amplitude $A = 0.1$ relative to a maximum of 0.5.

256 pulses of 4096 samples each at ADC output.

Out-of-band Gaussian noise dither with one-sided bandwidth $0.08 f_s$, and power level with RMS value at the quantization step size.

Processing in both dimensions with a −70 dB Taylor window, with nbar = 11.

The range-Doppler map without any mitigation is illustrated in Figure 25, and exhibits a peak harmonic spur level of –52 dBc. Note that a number of spurs occur at the same range, but different Doppler locations.

5.1 Reduce or Eliminate the Spurious Energy

The harmonic spurs are a function of the linearity of the ADC conversion process. Harmonic spurs can be reduced by selecting a more linear ADC component. The important parameter is INL with respect to full scale. This can be reduced by selecting a part with the same number of bits but better INL spec, or sometimes by selecting a part with more bits even if the INL relative to the LSB increases (gets worse) somewhat.

In principle, one might presume that INL can be characterized and compensated in the data. In practice, anecdotal evidence suggests that this is difficult and somewhat unreliable. Several reasons for this exist. These include

- Many high-speed ADC components multiplex the conversion to multiple internal ADC functional blocks. These internal ADC functional blocks have independent INL characteristics. It becomes somewhat problematic to assure that the right compensation goes to the right data sample.

- INL is somewhat temperature sensitive. Calibration is somewhat 'tricky' and would have to be done in-flight as temperature changes.

- A correction would require extending the internal busses inside the subsequent digital processors.

5.2 Move the Spurious Energy

Since INL generated harmonic spurs can exist anywhere in the overall range-Doppler map, moving some spurs outside the region of interest risks moving other harmonic spurs into the region of interest. Consequently, this is a nonviable mitigation strategy.

But not so fast…

If we can observe the spurs moving when the signal remains stationary, then we can identify the spurs, and perhaps neutralize them. We discuss this in somewhat more detail later.

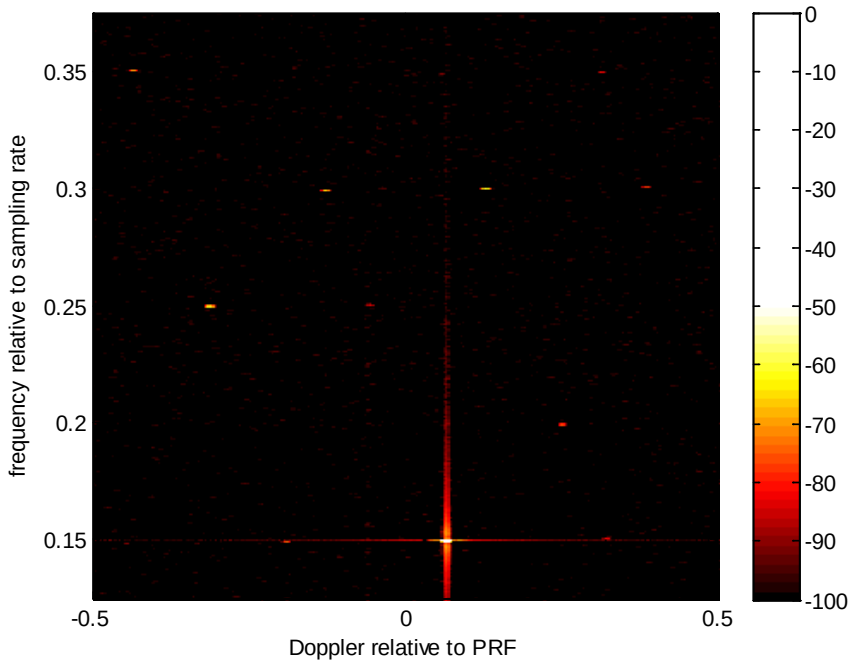

Figure 25. Range-Doppler map with INL induced harmonic spurs. The colorbar denotes dBc.

5.3 Smear the Spurious Energy

The most practical means of smearing the spurious energy is via phase modulation. Phase modulation is applied to the signal before the ADC conversion, and then removed from the data after conversion. Note that phase modulated harmonics in the data will be multiplied by the harmonic number, thereby multiplying the amount of phase modulation as well. Consequently, we can expect the amount of smearing to be harmonic dependent.

The kinds of phase modulation considered here are the same as were considered for I/Q balance in an earlier report.[9]

5.3.1 Range Smearing

A quadratic phase modulation in the fast-time, or range dimension will smear the harmonic spurs in range. A quadratic phase modulation is accomplished by a residual chirp. Figure 26 illustrates the effects of a residual chirp with Time-Bandwidth product of 20. The peak harmonic spur is at −68 dBc. This represents a 16 dB reduction.

5.3.2 Doppler Smearing

Doppler smearing may be accomplished by several convenient means.

A Doppler chirp with Time-Bandwidth product of 20 was applied for the example of Figure 27. The peak harmonic spur is at −68 dBc.

Random phase modulation on a pulse to pulse basis was applied for the example of Figure 28. The peak harmonic spur is at −67 dBc.

Random $0/\pi$ phase modulation on a pulse to pulse basis was applied for the example of Figure 29. The peak harmonic spur is at −52 dBc. Note that only odd-order harmonics are smeared. Even-order harmonics are unaffected by random $0/\pi$ phase modulation. Consequently, random $0/\pi$ phase modulation is better than nothing, but not by much.

5.3.3 Range and Doppler Smearing

Figure 30 illustrates the effects of using both a residual chirp with Time-Bandwidth product of 20, and a Doppler chirp with Time-Bandwidth product of 20. The peak harmonic spur is at −78 dBc. Together, these modulations effect a 26 dB improvement (reduction) in peak harmonic spur energy.

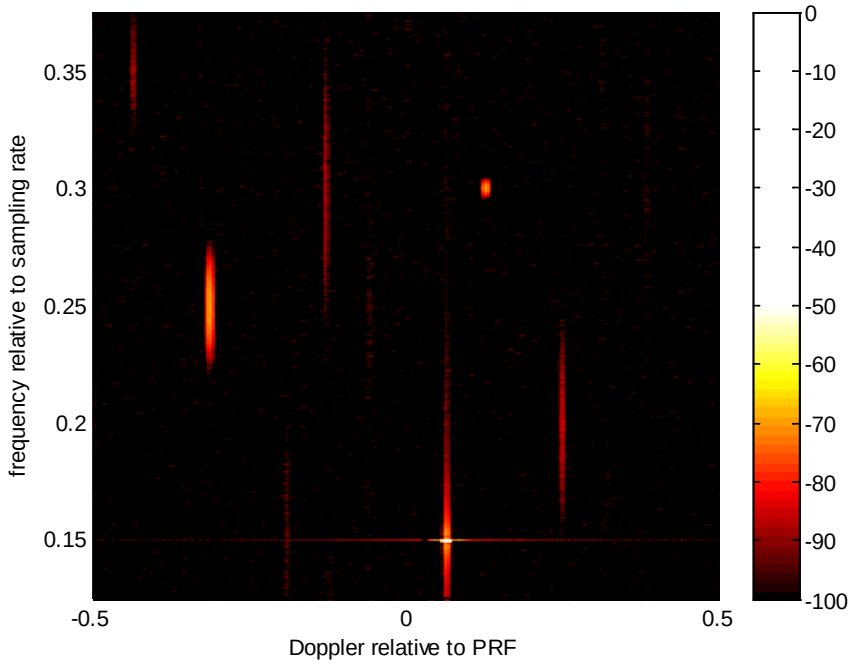

Figure 26. Range-Doppler map with INL induced harmonic spurs smeared in range by a residual chirp. The colorbar denotes dBc.

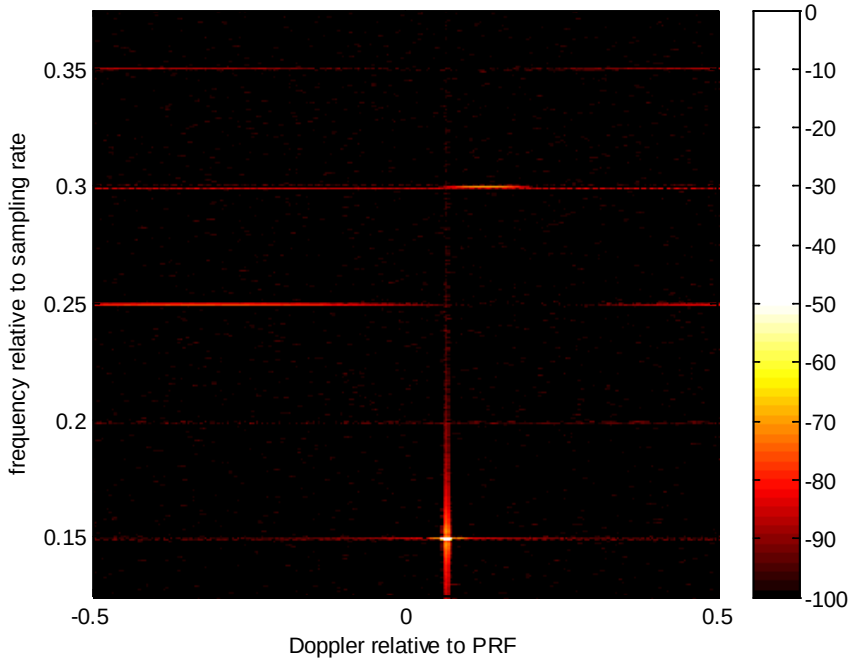

Figure 27. Range-Doppler map with INL induced harmonic spurs smeared by a Doppler chirp. The colorbar denotes dBc.

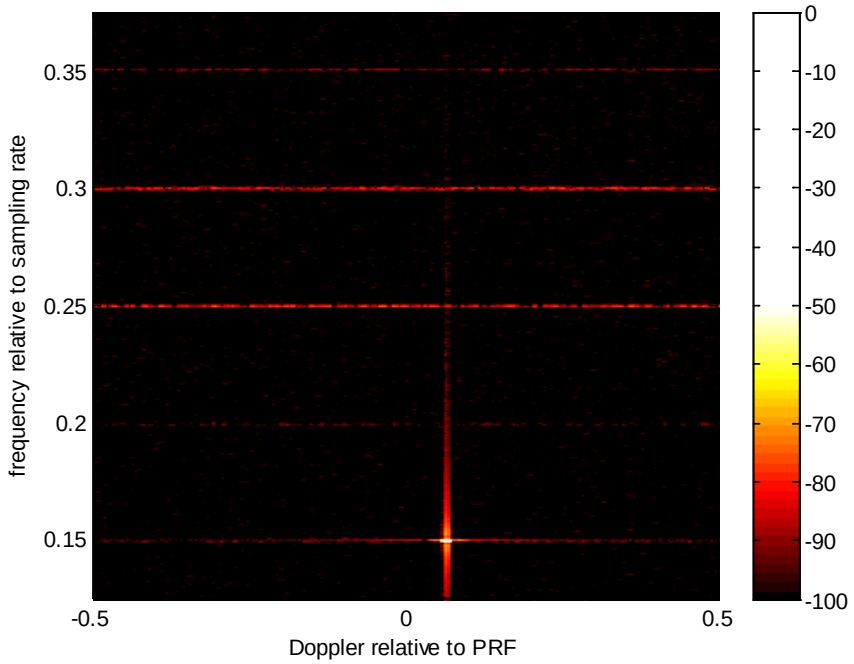

Figure 28. Range-Doppler map with INL induced harmonic spurs smeared by a pulse-to-pulse random phase modulation. The colorbar denotes dBc.

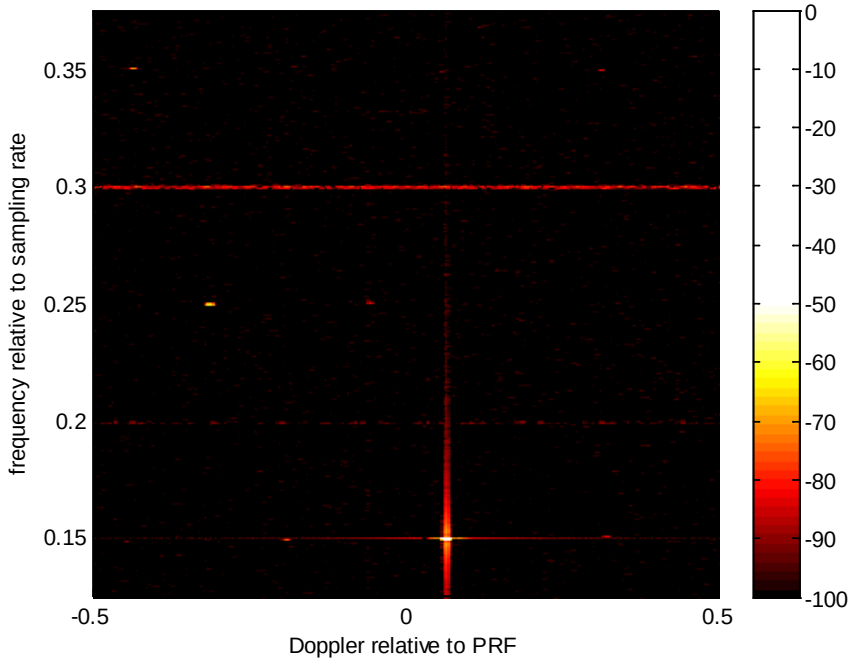

Figure 29. Range-Doppler map with INL induced harmonic spurs smeared by a pulse-to-pulse random 0/π phase modulation. The colorbar denotes dBc.

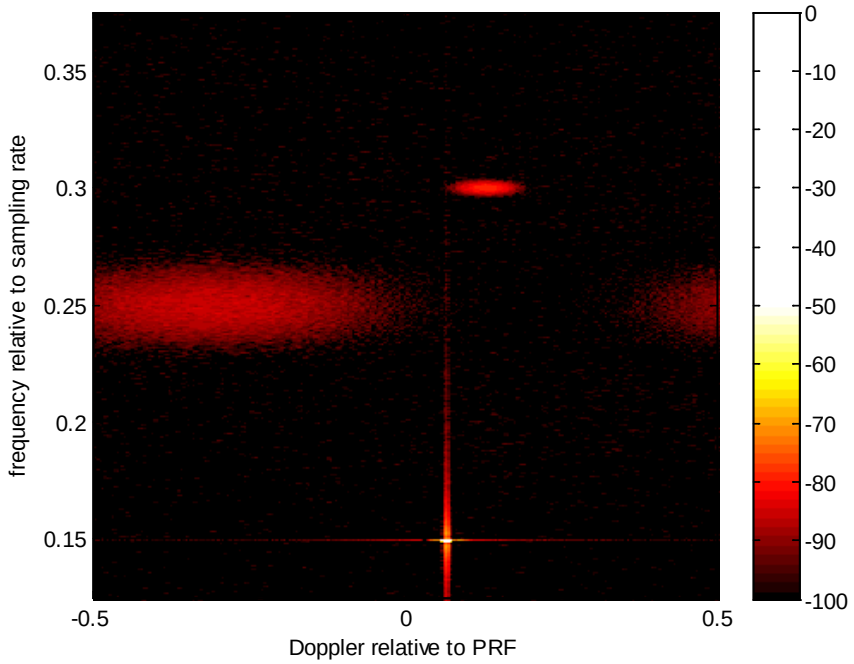

Figure 30. Range-Doppler map with INL induced harmonic spurs smeared by a residual range chirp and a Doppler chirp. The colorbar denotes dBc.

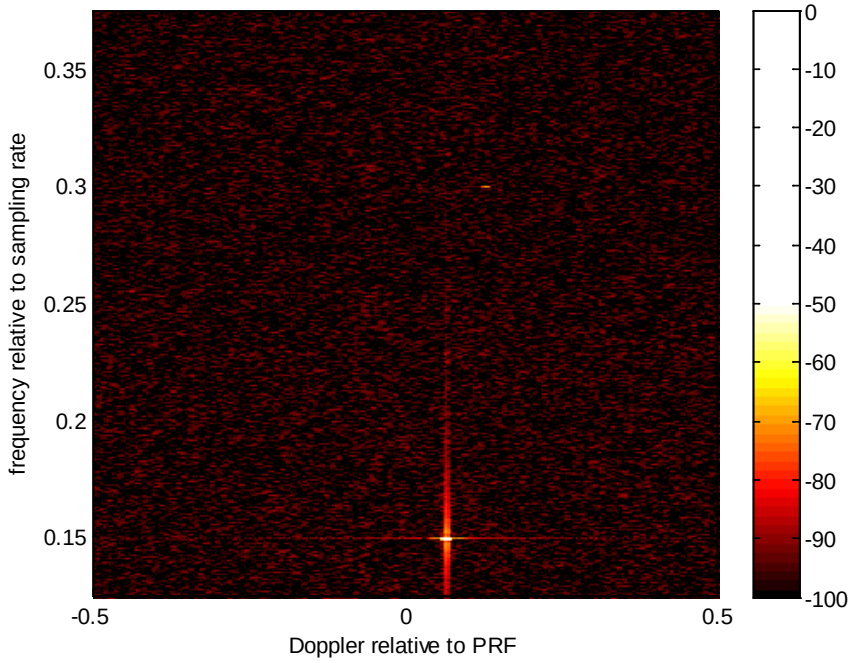

Figure 31. Range-Doppler map with INL induced harmonic spurs smeared by an elevated dither. The colorbar denotes dBc.

5.3.4 Dither

Another technique to 'spread' the imbalance energy is to employ a dither signal.[10] This involves adding noise with an RMS level that is substantially greater than the nominal quantization step size. Figure 31 illustrates the effects of using an out-of-band noise dither with RMS level at 16 times the quantization level. The peak harmonic spur is at –68 dBc.

A down side to this technique is that the dynamic range of the ADC itself is reduced somewhat by this additive elevated noise dither.

5.4 Range-Doppler Image Post-Processing

In GMTI modes, harmonic spurs are particularly problematic when they are large enough to be detected as false alarms. Consequently, if a particular detection can be identified as a harmonic spur, then it can be discounted as an errant detection, and not reported or processed further.

One way this can be accomplished is by identifying particularly strong target responses in the range-Doppler map, and then calculating where harmonic spurs 'ought' to occur, for some number of harmonics. The detection algorithm might then be desensitized at these locations, at least sufficiently so as to not allow a false alarm.

Of course problems with this are several. Among them, desensitizing the detection algorithm will also reduce the probability of detection for real targets. Additionally, typical INL specifications will generally cause a very large number of harmonic spurs that can generally be all over the range-Doppler map. Consequently, there will be a whole lot of desensitizing going on, more so yet for urban scenes that might have a large number of clutter discretes.

The bottom line is that resolving problematic INL effects in the range-Doppler map via post-processing is expected to be difficult with low probability of achieving acceptable results.

More recently, a spur apodization technique has been reported that shows promise, where a signal is processed simultaneously in two or more receiver channels with different modulations applied, undergoing simultaneous conversion in two or more ADCs. Modulations are chosen such that spur locations are expected to be different in the two channels even after target signal locations are registered. Consequently spur responses can be identified and mitigated.[11]

“It's not perfection that makes you beautiful, It's your imperfections”
— Peyton J Glenn

6 Recommendations for Radar Systems

Mitigating the effects of INL in radar systems can be divided into two principal realms.

1. Mitigation techniques for new radar designs. This allows us to touch hardware, firmware, and software.

2. Mitigation techniques to be retrofit into existing designs. We address this by limiting our attention to software solutions only.

We note that many of the recommendations for mitigating INL harmonic spurs also address other potential problems, such as I/Q imbalance effects.[9] In fact, other sources of nonlinear channel characteristics can be herewith addressed as well. We will concern ourselves mainly with GMTI operation.

6.1 New Designs

For new designs we recommend the following strategy.

- An ADC should be selected with excellent INL characteristics.

- Range smearing should be employed using a residual chirp with time-bandwidth product limited to a few percent of the range extent of the range swath.

- Doppler smearing should be employed using a true pulse-to-pulse phase modulation. Doppler smearing should be over an extent that is at least half the Doppler space before any presumming (in SAR) takes place. Modulation should be either a quadratic phase, or a true random phase with at best very fine quantization.

- Where practical, spur apodization might be considered in place of smearing.

6.2 Retrofit to Existing Designs

For retrofitting existing designs we recommend the following strategy.

- Range smearing should be employed using a residual chirp with time-bandwidth product limited to a few percent of the range extent of the range swath.

- Doppler smearing should be employed using a true pulse-to-pulse phase modulation. Doppler smearing should be over an extent that is at least half the Doppler space before any presumming (in SAR) takes place. Modulation should be either a quadratic phase, or a true random phase with at best very fine quantization.

“Being Normal is an Imperfection”
— Lily Battista

7 Conclusions

We reiterate the following points.

- ADC INL generates harmonic spurs.
- Harmonic spurs manifest as false targets in range-Doppler maps. If strong enough, they may generate false alarms in GMTI radar modes.
- Different ADCs have different INL characteristics. Lower INL characteristics are better. However, the specific harmonic content is also important. Clear 'preferred' ADC components exist.
- Mitigation techniques exist that require various radar parameter manipulations. These can substantially reduce harmonic spurs' peak levels by smearing them in range, Doppler, or both. These may even be retrofit into existing radar systems via software.
- Newer GMTI modes may require a full arsenal of techniques, even with the best ADC components.
- Many of the mitigation steps for addressing INL effects can be used to combat effects of other system channel nonlinearities as well, such as I/Q imbalance.

“The renowned seventh-century Zen master Seng-tsan taught that true freedom is being "without anxiety about imperfection.”
— Tara Brach, Radical Acceptance: Embracing Your Life With the Heart of a Buddha

References

[1] Walt Kester, “ADC Input Noise: The Good, The Bad, and The Ugly. Is No Noise Good Noise?”, Analog Dialogue 40-02, February 2006.

[2] William J. Caputi, Jr., “Stretch: A Time-Transformation Technique”, *IEEE Transactions on Aerospace and Electronic Systems*, Vol. AES-7, No. 2, pp 269-278, March 1971.

[3] “INL/DNL Measurements for High-Speed Analog-to-Digital Converters (ADCs)”, Application Note 283, Maxim Integrated Products, Inc., Sept. 1, 2000.

[4] Brad Brannon, Rob Reeder, “Understanding High Speed ADC Testing and Evaluation”, Analog Devices Application Note AN-835.

[5] Bert Tise, Dale Dubbert, “Digital intermediate frequency receiver module for use in airborne SAR applications,” US Patent 6,864,827, March 8, 2005.

[6] Armin W. Doerry, “Performance Limits for Exo-Clutter Ground Moving Target Indicator (GMTI) Radar”, Sandia Report SAND2010-5844, Unlimited Release, September 2010.

[7] A. W. Doerry, D. L. Bickel, A. M. Raynal, “Some comments on performance requirements for DMTI radar,” SPIE 2014 Defense & Security Symposium, Radar Sensor Technology XVIII, Vol. 9077, Baltimore MD, 5–9 May 2014.

[8] Armin W. Doerry, “Clutter in the GMTI Range-Velocity Map”, Sandia Report SAND2009-1797, Unlimited Release, April 2009.

[9] Armin W. Doerry, “Mitigating I/Q Imbalance in Range-Doppler Images,” Sandia Report SAND2014-2252, Unlimited Release, March 2014.

[10] Brad Brannon, “Overcoming Converter Nonlinearities with Dither”, Analog Devices Application Note AN-410, E2096–12–12/95.

[11] Armin W. Doerry, Douglas L. Bickel, “Apodization of Spurs in Radar Receivers Using Multi-Channel Processing,” Sandia Report SAND2014-1678, Unlimited Release, March 2014.

Distribution

Unlimited Release

1	MS 0519	J. A. Ruffner	5349	
1	MS 0519	A. W. Doerry	5349	
1	MS 0519	L. Klein	5349	
1	MS 0532	J. J. Hudgens	5240	
1	MS 0532	B. L, Tise	5348	
1	MS 0533	D. F. Dubbert	5345	
1	MS 0899	Technical Library	9536	(electronic copy)


Sandia National Laboratories